DISCONTINUOUS GALERKIN METHODS FOR COMPRESSIBLE MISCIBLE DISPLACEMENTS AND APPLICATIONS IN RESERVOIR SIMULATION

By

Yue Kang

A DISSERTATION

Submitted in partial fulfillment of the requirements for the degree of

DOCTOR OF PHILOSOPHY

In Mathematical Sciences

MICHIGAN TECHNOLOGICAL UNIVERSITY

2024

This dissertation has been approved in partial fulfillment of the requirements for the Degree of DOCTOR OF PHILOSOPHY in Mathematical Sciences.

Department of Mathematical Sciences

Dissertation Advisor:	*Dr. Yang Yang*
Committee Member:	*Dr. Zhengfu Xu*
Committee Member:	*Dr. Alexander E. Labovsky*
Committee Member:	*Dr. Qingli Dai*
Department Chair:	*Dr. Jiguang Sun*

Contents

List of Figures

List of Tables

Preface

This dissertation contains published and in-processing works completed by the author of this dissertation. The contributions of the author are detailed in the following paragraphs.

In the second chapter, the author has collaborated with Wengjing Feng, Hui Guo and Yang Yang. The main author's work is proving the second-order accuracy of the numerical scheme in the time discretization and software implementation. The work has been published in the Journal of Computational Physics. This work was supported by the Fundamental Research Funds for the Central Universities 20CX05011A and the Major Scientific and Technological Projects of CNPC under Grant ZD2019-183-008 and NSF grant DMS-1818467.

In the third chapter, the author collaborated with Tao Xiong and Yang Yang. The main author's work involves coding the oscillation-free discontinuous Galerkin methods with high order implicit pressure explicit concentration time matching for simulating viscous fingering instabilities and drafting the manuscript. This work is supported in part by the Simons Foundation 961585.

Acknowledgments

I extend my sincere gratitude to my advisor, Dr. Yang Yang, for his invaluable advice and unwavering support. Dr. Yang has provided numerous opportunities, inspiration, encouragement, patience, and guidance throughout my research and my journey as a graduate student.

I would also like to express my thanks to the committee members, Dr. Zhengfu Xu, Dr. Alexander E. Labovsky, and Dr. Qingli Dai, for their insightful advice, which has significantly contributed to the completeness of this work.

Special appreciation goes to Dr. Jiguang Sun, the Department chair, for granting me the opportunity to teach. I am grateful to Ann Humes, Debra Zei, and Jason Gregersen, who served as coordinators and mentors in my teaching endeavors.

Furthermore, I extend my thanks to Tessa Kriz, Yasasya Batugedara Mohottalalage, Patrick McFall, Jacob Blazejewski, Xing Ling and Zhiyuan Lu whose contributions have greatly facilitated my life as a graduate student in the department. My sincere appreciation also goes to Ziyao Xu, for his willingness to answer all my questions and engage in helpful discussions.

Additionally, I would like to express my gratitude to my husband, Chen Zhao, for guiding me towards achieving my ultimate goals, and to my family and friends who have provided encouragement and support in both academic and non-academic pursuits.

Abstract

This dissertation contains research on discontinuous Galerkin (DG) methods applied to the system of compressible miscible displacements, which is widely adopted to model surfactant flooding in enhanced oil recovery (EOR) techniques. In most scenarios, DG methods can effectively simulate problems in miscible displacements. However, if the problem setting is complex, the oscillations in the numerical results can be detrimental, with severe overshoots leading to nonphysical numerical approximations. The first way to address this issue is to apply the bound-preserving technique. Therefore, we adopt a bound-preserving Discontinuous Galerkin method with a Second-order Implicit Pressure Explicit Concentration (SIPEC) time marching method to compute the system of two-component compressible miscible displacement in our first work. The Implicit Pressure Explicit Concentration (IMPEC) method is one of the most prevalent time marching approaches used in reservoir simulation for solving coupled flow systems in porous media. The main idea of IMPEC is to treat the pressure equation implicitly and the concentration equations explicitly. However, this treatment results in a first-order accurate scheme. To improve the order of accuracy of the scheme, we propose a correction stage to compensate for the second-order accuracy in each time step, thus naming it the SIPEC method. The SIPEC method is a crucial innovation based on the traditional second-order strong-stability-preserving Runge-Kutta (SSP-RK2) method. However, the SIPEC method is limited

to second-order accuracy and cannot efficiently simulate viscous fingering phenomena. High-order numerical methods are preferred to reduce numerical artifacts and mesh dependence. In our second work, we adopt the IMPEC method based on the implicit-explicit Runge-Kutta (IMEX-RK) Butcher tableau to achieve higher order temporal accuracy while also ensuring stability. The high-order discontinuous Galerkin method is employed to simulate the viscous fingering fluid instabilities in a coupled nonlinear system of compressible miscible displacements. Although the bound-preserving techniques can effectively yield physically relevant numerical approximations, their success depends heavily on theoretical analysis, which is not straightforward for high-order methods. Therefore, we introduce an oscillation-free damping term to effectively suppress the spurious oscillations near discontinuities in high-order DG methods. As indicated by the numerical experiments, the incorporation of the bound-preserving DG method with SIPEC time marching and high-order OFDG with IMPEC time marching provides satisfactory results for simulating fluid flow in reservoirs.

Chapter 1

Introduction

Numerical modeling of miscible displacements within porous media is pivotal for overcoming obstacles in oil recovery and mitigating environmental pollution. This intricate issue encompasses a system of interlinked nonlinear partial differential equations, demanding precise and reliable simulations. The complexity of these equations drives numerical analysts to persistently seek innovative solutions and methodologies capable of adeptly navigating the nuances of this coupled system.

The foundational work on miscible displacements in porous media was established through the pioneering application of mixed finite element methods, as introduced in the seminal papers by Douglas et al. [1, 2]. This foundational research laid the groundwork for further exploration into the compressible aspects of the problem,

detailed in [3]. The development of new numerical strategies, such as the finite difference method [4], the splitting positive definite mixed element method [5], and the H1-Galerkin mixed method [6], marked significant advancements in the field. In an innovative approach, an Eulerian-Lagrangian localized adjoint method was integrated with a mixed finite element method for solving the transport and pressure equations respectively [7]. Kumar's development of a mixed and discontinuous finite volume method specifically for incompressible miscible displacement issues [8], along with the introduction of a discrete duality finite volume (DDFV) scheme by Hillairet et al. [9]—focusing on scheme convergence—highlighted the ongoing evolution of methodologies addressing these complex problems. Recent years have seen the Discontinuous Galerkin (DG) methods gain prominence for their effectiveness in handling compressible miscible displacements [10, 11, 12, 13, 14], with particular attention to managing numerical approximation jumps and the non linearity of the convection term. The breadth of research on DG methods for incompressible miscible displacements further emphasizes their importance, with significant contributions made by Bartels et al., Guo, Kumar, Riviere, Sun, and Wheeler among others [8, 15, 16, 17, 18, 19]. A notable method in this domain is the interior penalty DG (IPDG) method, widely applied for convection-diffusion and elliptic equations [17], showcasing the diversification and specialization within numerical techniques to tackle the challenges of modeling miscible displacements in porous media.

While the methods previously discussed are generally effective for simulating miscible

displacements, challenges arise in complex scenarios, such as fluid flow around obstacles, where numerical oscillations can detrimentally impact results. As highlighted in [20], direct numerical simulations in such cases may produce severe overshoots, leading to unphysical numerical approximations. To mitigate these issues, the bound-preserving technique emerges as a primary solution. Specifically, the second-order bound-preserving technique for convection-diffusion equations has been investigated [21], showing applicability to various DG methods, including IPDG, local DG, and ultra-weak DG, as evidenced in [22, 23]. However, extending these techniques to higher-order schemes presents significant challenges. Notably, the development of the third-order MPP scheme for LDG methods on overlapping meshes and the DDG method are discussed in [24, 25], alongside other high-order methods that involve adjustments to numerical fluxes [26, 27, 28]. However, the previous studies mentioned above have given little attention to bound-preserving techniques for miscible displacements. In many practical scenarios, physical parameters are closely linked to the concentration c. If c falls outside the interval 0 to 1, we may not obtain the parameters used in the system, and in extreme cases, the numerical approximations may become unstable. In [23], Guo and Yang first proposed bound-preserving DG methods for the coupled system of two-component compressible miscible displacements. The core idea is as follows: (1) Enforce $c_1 + c_2 = 1$ by selecting consistent numerical fluxes in the schemes of the pressure and concentration equations. (2) Derive the scheme

of the second component concentration by subtracting the scheme of the concentration equation from that of the pressure equation. (3) Apply positivity-preserving techniques to both c_1 and c_2 separately. The authors theoretically demonstrated in [23] that this algorithm can produce physically relevant numerical cell averages. A slope limiter can then be employed to ensure that the numerical approximations stay within the desired bounds. Later, in [29], the authors expanded this idea to multi-component miscible displacements, proposing high-order bound-preserving DG methods on triangular meshes and showing that the slope limiter does not affect accuracy. Bound-preserving finite difference methods were also explored in [30]. Several other extensions following this approach can be found in [31, 32, 33].

Bound-preserving techniques, crucial for ensuring physical accuracy in numerical simulations of miscible displacements in porous media, often rely on strong-stability-preserving Runge-Kutta (SSP-RK) time discretizations [34, 35, 36, 37]. Despite their effectiveness, these techniques necessitate small time steps, significantly increasing computational costs and limiting their applicability across various scenarios. The necessity for small time steps primarily stems from the heterogeneity of the media, where areas of high permeability lead to substantial diffusion coefficients in the pressure equation, as explored in [38] and accompanying studies. To navigate these challenges, one strategy involves adopting implicit formulations for the pressure equation while maintaining an explicit approach for the concentration equation, given the

formidable complexity of fully implementing implicit schemes. Although fully implicit schemes, as described in [39, 40], guarantee unconditional stability, they demand extensive computational effort at each time step due to the system's thorough coupling. In response, the IMplicit Pressure Explicit Concentration (IMPEC) scheme [41, 42, 43, 44, 45] has emerged as a favored alternative for modeling compressible flows in porous media. This approach, which processes the pressure equation implicitly and the concentration equation explicitly, simplifies system configuration, enhances execution efficiency, and reduces memory requirements per time step by decoupling the equations and solving them sequentially. Originally introduced by Sheldon et al. [46] and further developed by Stone et al. [47], the IMPEC method has evolved to include a fully mass-conservative iterative version for multi-component compressible flow [48]. Despite these advancements, IMPEC methods generally achieve only first-order time accuracy. Developing a second-order IMPEC time method that remains compatible with bound-preserving techniques presents a significant technical challenge, underscoring the ongoing need for innovative solutions in the numerical modeling of porous media flows

In Chapter 2, we construct a Second-order IMplicit Pressure Explicit Concentration (SIPEC) time method with the bound-preserving technique for Darcy compressible miscible displacements. The method consists of three steps: (1) Using the SSP-RK2 method, the pressure equation is treated implicitly and the concentration equation is treated explicitly to obtain a first-order time scheme. (2) The local truncation

error of the first-order scheme is derived. (3) In accordance with the method outlined in [49], a corrective stage is introduced to offset the second-order accuracy of the aforementioned scheme and simultaneously uphold the bound-preserving nature of the numerical cell averages. In Section 2.5, some numerical experiments and results will be shown to demonstrate the accuracy and capability of the bound-preserving IPDG methods coupled with the SIPEC time discretization.

The SIPEC method, as detailed in [50, 51], achieves second-order accuracy but falls short in efficiently simulating complex phenomena such as viscous fingering. Comparative analyses in Section 3.5 between second-order and higher-order schemes underscore the importance of advanced methodologies. While bound-preserving techniques are instrumental in generating physically plausible numerical approximations, their implementation, particularly for high-order methods, demands rigorous theoretical underpinning a challenge not readily addressed by the strategies proposed in [50, 51] for extending to third-order accuracy. To mitigate spurious oscillations near discontinuities in high-order Discontinuous Galerkin (DG) methods, the development of various limiters, including the *minmod*-type Total Variation Diminishing (TVD) limiter, the Total Variation Bound (TVB) limiter, and the Weighted Essentially Non-Oscillatory (WENO) limiter, has been pivotal, as discussed in [52, 53, 54]. These limiters fine-tune the numerical solution post-calculation by identifying and processing troubled cells, although their effectiveness can vary with the specific problem at hand, potentially affecting the desired attributes of the original schemes. An

alternative strategy involves embedding artificial terms into the weak formulation to achieve properties like entropy stability or shock capturing capabilities, as explored in [55]. However, the success of artificial diffusion methods hinges on the precise adjustment of parameters, which, if improperly calibrated, can either excessively smear shocks or fail to adequately dampen spurious oscillations. A novel approach introduced by Liu [56] offers a different solution to addressing numerical oscillations in DG methods by incorporating a damping term into the standard DG framework. This method employs a uniform selection of damping coefficients to ensure minimal impact in smooth solution regions while effectively dampening oscillations near discontinuities, thus obviating the need for problem-specific parameter tuning and simplifying implementation. In light of these developments, the Optimized Flux Discontinuous Galerkin (OFDG) methods, as demonstrated in [57], have been applied successfully to multi-component chemically reacting flows. These methods not only conserve mass and adhere to bound-preserving principles but also outperform traditional DG schemes with TVD limiters in numerical experiments. This advancement motivates the exploration of OFDG methods as a viable solution for addressing oscillations and developing IMPEC methods tailored for miscible displacement scenarios.

In Chapter 3, we introduce an advanced conservative high-order interior penalty Discontinuous Galerkin (DG) scheme, augmented with an oscillation-free damping term

(OFDG), designed for compressible miscible displacements. This scheme incorporates a high-order Implicit-Explicit (IMEX) Runge-Kutta [58] approach for time discretization. The core advantage of this high-order IMPEC method lies in its ability to combine high-order temporal accuracy with the utilization of larger time-step sizes, significantly reducing computational demands. We validate the effectiveness, robustness, and accuracy of this fully integrated DG method, featuring an oscillation-free damping term, through simulations conducted on a rectangular mesh. Specifically, in Section 3.5, we showcase successful simulations of the viscous fingering instability phenomenon, employing high-order oscillation-free DG schemes to highlight their capability in capturing complex flow dynamics accurately.

Chapter 2

Bound-preserving DG methods with second-order implicit pressure explicit concentration time marching for compressible miscible displacements in porous media

In this paper, we construct bound-preserving interior penalty discontinuous Galerkin (IPDG) methods with a second-order implicit pressure explicit concentration (SIPEC)

time marching for the coupled system of two-component compressible miscible displacements. The SIPEC method is a crucial innovation based on the traditional second-order strong-stability-preserving Runge-Kutta (SSP-RK2) method. The main idea is to treat the pressure equation implicitly and the concentration equation explicitly. However, this treatment would result in a first-order accurate scheme. Therefore, in all previous works, only the combination of forward and backward Euler time integration was considered. In this paper, we propose a correction stage to compensate for the second-order accuracy in each time step. There are two main difficulties in constructing a second-order scheme. Firstly, in the concentration equation, correction of the diffusion term will cause anti-diffusion, leading to malfunction of the bound-preserving technique. We can deal with the velocity in the diffusion term explicitly to avoid correction of the diffusion term. Secondly, we need to ensure that the bound-preserving technique for the convection and source terms can be applied when the correction stage has been established. In fact, in the correction stage, the new approximation to the concentration can be chosen as the numerical solution in the previous stage, so the numerical cell averages are positivity-preserving. Moreover, we use the same correction technique for the pressure, so that the consistent flux pairs would guarantee the preservation of the upper bound 1 of the concentration. Numerical experiments will be given to demonstrate that the proposed scheme can reduce the computational cost significantly compared with explicit schemes if the diffusion coefficient D is small in the concentration equation. Moreover, the proposed method

also yields much larger cfl number compared with first-order implicit pressure explicit concentration schemes. Moreover, the effectiveness of the bound-preserving technique will also be presented.

Keywords: Compressible miscible displacements; Interior penalty discontinuous Galerkin method; Second-order implicit pressure explicit concentration method; Bound-preserving; Contaminant transportation

2.1 Introduction

Numerical simulation of miscible displacements in porous media is of great significance in oil recovery and contaminant transportation problems. The miscible displacements are usually described by a coupled system of nonlinear partial differential equations. There is a great demand for the accuracy and efficiency of the numerical methods for the coupled system. In this paper, we consider the fluid mixture with two components, and the classical equations governing the compressible miscible displacements on the computational domain $\Omega = [0, 2\pi] \times [0, 2\pi]$ for all $(x, y) \in \Omega, 0 < t \leq T$ are as follows:

$$d(c)\frac{\partial p}{\partial t} + \nabla \cdot \mathbf{u} = d(c)\frac{\partial p}{\partial t} - \nabla \cdot \left(\frac{\kappa(x,y)}{\mu(c)}\nabla p\right) = q, \tag{2.1}$$

$$\phi\frac{\partial c}{\partial t} + b(c)\frac{\partial p}{\partial t} + \mathbf{u} \cdot \nabla c - \nabla \cdot (\mathbf{D}\nabla c) = (\tilde{c} - c)q. \tag{2.2}$$

Here the unknown variables p, $\mathbf{u}$ and c are the pressure of the fluid mixture, the Darcy velocity of the mixture, and the volumetric concentration of interested species, respectively. ϕ and κ are the porosity and permeability of the rock, respectively. μ is concentration-dependent viscosity. q is the external volumetric flow rate, and $\tilde{c}$ is the concentration of the fluid in the external flow, which must be specified at points where injection ($q > 0$) takes place, and is assumed to be equal to c at production points ($q < 0$). The diffusion coefficient $\mathbf{D}$ is symmetric and arises from two aspects: molecular diffusion, which is rather small for field-scale problems, and dispersion, which is velocity-dependent. It takes the form

$$\mathbf{D}(\mathbf{u}) = \phi(x, y)(d_{mol}\mathbf{I} + d_{long}|\mathbf{u}|\,\mathbf{E} + d_{tran}|\mathbf{u}|\,\mathbf{E}^{\perp}), \tag{2.3}$$

where $\mathbf{E}$ is a 2×2 matrix, representing the orthogonal projection along the velocity vector given as

$$(\mathbf{E}(\mathbf{u}))_{ij} = \frac{u_i u_j}{|\mathbf{u}|^2}, \quad 1 \le i, j \le 2,\ \mathbf{u} = (u_1, u_2)^T,$$

and $\mathbf{E}^{\perp} = \mathbf{I} - \mathbf{E}$ is the orthogonal complement. The diffusion coefficient d_{long} measures the dispersion in the direction of the flow and d_{tran} shows that transverse to the flow. To ensure the stability of the scheme, $\mathbf{D}$ is assumed to be strictly positive definite in almost all the previous works. In this paper, $\mathbf{D}$ is assumed to be positive semi-definite. Therefore, we have $D_{11} \ge 0$, $D_{22} \ge 0$, and $D_{12} = D_{21}$. Moreover, the

pressure is uniquely determined up to a constant, thus we assume $\int_\Omega p dxdy = 0$ to ensure the uniqueness. However, this assumption is not essential. Other coefficients can be stated as follows:

$$c = c_1 = 1 - c_2, \quad d(c) = \phi \sum_{j=1}^{2} z_j c_j, \quad b(c) = \phi c_1 \left\{ z_1 - \sum_{j=1}^{2} z_j c_j \right\},$$

where c_j and z_j are the concentration and the compressibility factor of the jth component of the fluid mixture, respectively. In this paper, we consider homogeneous Neumann boundary conditions

$$\mathbf{u} \cdot \mathbf{n} = 0, \quad (\mathbf{D}\nabla c - c\mathbf{u}) \cdot \mathbf{n} = 0, \tag{2.4}$$

where $\mathbf{n}$ is the unit outer normal of the boundary $\partial\Omega$. Moreover, the initial solutions are given as

$$c(x, y, 0) = c_0(x, y), \quad p(x, y, 0) = p_0(x, y), \quad (x, y) \in \Omega.$$

In the previous works, Douglas et al. [1, 2] first proposed the mixed finite element method for miscible displacements in porous media, and carried out the follow-up study in [3]. Later, in [59], Chou and Li gave the optimal order estimates in L^2-norm and almost optimal order estimates in L^∞-norm. Subsequently, various numerical methods were introduced to obtain better approximations, such as the finite difference

method [4, 60, 61], splitting positive definite mixed element method [5], characteristic finite element method [62] and H^1-Galerkin mixed method [63]. Besides the above, Wang et al. studied an accurate and efficient simulator for problems with wells in [6]. Later, the authors introduced an Eulerian-Lagrangian localized adjoint method to solve the transport equation for concentration, and a mixed finite element method to solve the pressure equation [7]. Moreover, Kumar [8] developed a mixed and discontinuous finite volume method for incompressible miscible displacement problems. In [9], a DDFV scheme was proposed to solve the problem, where the convergence of the scheme was studied.

Recently, the discontinuous Galerkin (DG) methods have been widely used to solve the compressible miscible displacements [10, 11, 12, 13, 64, 65] and incompressible miscible displacements [15, 16, 18, 19, 66, 67] in porous media. The methods, first introduced in [68], employ finite element spaces containing elementwise discontinuous functions and develop special numerical techniques to control the jumps of numerical approximations as well as the nonlinearity of the convection term. Therefore, DG methods have the advantages of good stability, high order accuracy, flexibility on h-p adaptivity and on complex geometry, and gained great popularity. A commonly used DG method for convection-diffusion equations and elliptic equations is the interior penalty DG (IPDG) method [17].

As another important aspect of the DG methods, the bound-preserving technique has

been widely studied. In [69], Zhang and Shu first constructed the genuinely maximum-principle-satisfying high order DG and finite volume methods. Subsequently, this bound-preserving technique has been successfully extended to many problems, such as compressible Euler equations [70, 71], hyperbolic equations involving δ-singularities [72, 73, 74], relativistic hydrodynamics [75] and shallow water equations [76], etc. If the exact solution has only one lower bound 0, then the technique is also called positivity-preserving technique. For convection-diffusion equations, the second-order bound-preserving technique has been studied in [77]. The technique works for IPDG, local DG and ultra-weak DG methods, see [22, 23] for some applications. However, the extension to high-order schemes seems to be not straightforward. The third-order MPP scheme based on LDG methods on overlapping meshes [78] and DDG method [25] were discussed. Other high-order methods were also investigated in [28, 79, 80] based on the modification of numerical fluxes. However, the previous works above paid little attention to the bound-preserving techniques for miscible displacements. In many actual problems, physical parameters are closely related to the concentration c. If c is placed out of the interval 0 to 1, we might not obtain the parameters used in the system, and the numerical approximations may blow up in some extreme cases [23]. We will demonstrate this point in numerical experiments in Section 2.5. In [23], two authors of this paper first proposed the bound-preserving DG methods for the coupled system of the two-component compressible miscible displacements.

The basic idea is as follows. (1) Enforce $c_1 + c_2 = 1$ by choosing consistent numerical fluxes (see Definition 2.2.1) in the schemes of the pressure and concentration equations. (2) Subtract the scheme of the concentration equation from that of the pressure equation to obtain that of the second component concentration. (3) Apply the positivity-preserving techniques to both c_1 and c_2, respectively. In [23], the authors theoretically proved that the above algorithm can yield physically relevant numerical cell averages. Then a slope limiter can be applied to make the numerical approximations to be within the desired bounds. Later, in [29], Chuenjarern et al. extended the idea to multi-component miscible displacements, proposed high-order bound-preserving DG methods on triangular meshes, and proved that the slope limiter does not affect the accuracy. The bound-preserving finite difference methods were also discussed in [30]. Some other extensions following the same idea can be found in [31, 32, 33]. Unfortunately, the above bound-preserving techniques are based on strong-stability-preserving Runge-Kutta (SSP-RK) time discretization [34, 35, 36, 37], which lead to small time step sizes and large computational cost. Therefore, those works can hardly be applied in practice. The main issue for the small time step size is due to the heterogeneity of the media, see e.g. [38] and the references therein. In fact, in some part of the media, the permeability would be extremely high, leading to large diffusion coefficients in the pressure equation. Therefore, a straightforward alternative is to consider implicit forms of the pressure equation. Moreover, the concentration equation should be solved explicitly as the fully implicit scheme would

be extremely difficult to implement. However, this implicit pressure explicit concentration (IMPEC) treatment would degenerate any high-order time integration to a first-order one [81], hence all the previous works mainly consider the combination of forward and backward Euler methods, see e.g. [45].

In this paper, we will use IPDG method for spatial discretization, develop a second-order implicit pressure explicit concentration (SIPEC) time discretization for compressible miscible displacements in porous media, and then apply bound-preserving techniques to obtain physically relevant numerical approximations. To be more precise, the IPDG method in this paper is in a symmetric form, i.e. symmetric interior penalty Galerkin method [82]. Furthermore, the SIPEC method is a crucial innovation in this paper, which is based on the traditional SSP-RK2 method. The basic idea can be divided into the following three steps. (1) Based on the framework of the SSP-RK2 method, we treat the pressure equation implicitly and the concentration equation explicitly so as to obtain a scheme that is only first-order accurate in time. (2) By comparing the above scheme with the traditional SSP-RK2 scheme, the truncation error between them is obtained. (3) Following [81], a correction stage is introduced to compensate for the second-order accuracy of the above scheme, maintaining the bound-preserving property of the numerical cell averages in the meantime. The bound-preserving technique for the fully-explicit schemes has been given in [23, 29], hence we only need to focus on the technique in the correction stage. However, we would like to emphasize that the time integration used in this paper is

totally different from the fully explicit methods used in [23, 29]. There are two main difficulties in constructing the correction stage. Firstly, it is very difficult to correct the diffusion term in the concentration equation, which will cause anti-diffusion and the bound-preserving techniques fail to work. Secondly, we need to ensure that the bound-preserving technique can be applied to the convection and source terms when the correction stage has been established. In fact, in the concentration equation, we treat the velocity and pressure in the convection and source terms implicitly while those in the diffusion term explicitly so as to avoid the correction of the diffusion term. We can theoretically prove that such correction will yield a second-order accuracy in time. Moreover, in the correction stage, the new approximation to the concentration can be chosen as the numerical solution in the previous stage, so the numerical cell averages are positive-preserving. Besides, the correction for pressure is designed in a similar way, which can preserve the upper bound of the cell averages of the concentration by using consistent numerical fluxes in the correction stage. In numerical experiments, we compare the SIPEC method with the SSP-RK2 method used in [23, 29]. The time accuracy of both methods is second-order. Moreover, the results show that the CPU time by the SIPEC method is significantly less than that by the SSP-RK2 method. In addition, we also compare the SIPEC method with the IMPEC method, where backward and forward Euler methods are used to discretize the time derivatives of pressure and concentration equations, respectively. The results show that there is no significant difference between the two methods when the time

step is small. However, we can observe strong oscillations if the time step is large in the IMPEC method, while the oscillations disappear for SIPEC method. This is because the concentration equation is discretized by the second-order IPDG method coupled with the first-order forward Euler time-marching scheme in IMPEC schemes, leading to instability if $\Delta t \sim \Delta x$. Since our method is based on the SSP-RK2 time integration, for stability, we only consider second-order spatial discretization. The case with high-order spatial discretization will be discussed in the future. Finally, we point out that if the diffusion coefficient D is small, the SIPEC method has a significant advantage compared with the traditional SSP-RK2 scheme in computational cost. However, if D is large, the advantage may not be significant.

The paper is organized as follows. In Section 2.2, we introduce the notations to be used throughout the paper, then construct the IPDG scheme for compressible miscible displacements. In Section 2.3, the SIPEC method is derived. The bound-preserving techniques will be given in Section 2.4. In Section 2.5, some numerical experiments and results will be shown to demonstrate the accuracy and capability of the bound-preserving IPDG methods coupled with the SIPEC time discretization. We will end in Section 2.6 with concluding remarks.

2.2 The semi-discrete IPDG scheme

In this section, we will introduce the notations to be used throughout the paper, then construct IPDG scheme for compressible miscible displacement problem (2.1)-(2.2), and demonstrate some key points.

2.2.1 Basic notations

We first introduce the notation used throughout the paper. We consider rectangular meshes only, and the case for triangular meshes can be obtained following [29] and the correction stage introduced in this paper. Let $0 = x_{\frac{1}{2}} < \cdots < x_{N_x+\frac{1}{2}} = 2\pi$ and $0 = y_{\frac{1}{2}} < \cdots < y_{N_y+\frac{1}{2}} = 2\pi$ be the coordinates of the grid points in the x and y directions, respectively. Define $I_i = (x_{i-\frac{1}{2}}, x_{i+\frac{1}{2}})$ and $J_j = (y_{j-\frac{1}{2}}, y_{j+\frac{1}{2}})$. Let $K_{ij} = I_i \times J_j,\ (i = 1, \ldots, N_x,\ j = 1, \ldots, N_y)$ be the i, j-th cell and denote $\Omega_h = \underset{i,j}{\cup} K_{ij}$ as a partition of Ω. Unless otherwise stated, we always use K to denote the cells. The mesh sizes in the x and y directions are given as $\Delta x_i = x_{i+\frac{1}{2}} - x_{i-\frac{1}{2}}$ and $\Delta y_j = y_{j+\frac{1}{2}} - y_{j-\frac{1}{2}}$, respectively. For simplicity, we assume uniform meshes and denote $\Delta x = \Delta x_i$ and $\Delta y = \Delta y_j$. However, this assumption is not essential. Moreover, we denote Γ to be the set of all element interfaces, and $\Gamma_0 = \Gamma \backslash \partial\Omega$. For any $e \in \Gamma$, denote $|e|$ to be the length of e. We choose $\boldsymbol{\beta} = (1, 1)^T$ to be a fixed vector that is not parallel to

any normal of the cell interfaces, and define $\mathbf{n}_e$ as the unit normal of $e \in \Gamma_0$ such that $\boldsymbol{\beta} \cdot \mathbf{n}_e > 0$. Furthermore, we denote $\partial\Omega_+ = \{e \in \partial\Omega : \boldsymbol{\beta} \cdot \mathbf{n} > 0\}$, where $\mathbf{n}$ is the unit outer normal of $\partial\Omega$, and $\partial\Omega_- = \partial\Omega \backslash \partial\Omega_+$. In this paper, we will construct a second-order IPDG scheme, and the finite element space is chosen as

$$W_h = \{z : z|_K \in Q^1(K),\ \forall K \in \Omega_h\},$$

where $Q^1(K)$ denotes the space of tensor product of linear polynomials in K. Moreover, let $e \in \Gamma_0$ be an interior edge shared by two elements K_ℓ and K_r, where $\boldsymbol{\beta} \cdot \mathbf{n}_\ell > 0$ and $\boldsymbol{\beta} \cdot \mathbf{n}_r < 0$ with $\mathbf{n}_\ell$ and $\mathbf{n}_r$ being the unit outer normal of K_ℓ and K_r. For any $z \in W_h$, z^- and z^+ represent the values taken from K_ℓ and K_r, respectively. Furthermore, we use $[z] = z^+ - z^-$ and $\{z\} = \frac{1}{2}(z^+ + z^-)$ as the jump and average of z at the cell interfaces, respectively. For simplicity, for any $e \in \partial\Omega_-$, we define $z^-|_e = 0$. Similarly, for any $e \in \partial\Omega_+$, we define $z^+|_e = 0$.

2.2.2 The semi-discrete IPDG scheme

To construct the IPDG scheme, the coupled system (2.1)-(2.2) is rewritten into the following conservative form:

$$d(c)\frac{\partial p}{\partial t} + \nabla \cdot \mathbf{u} = q, \tag{2.1}$$

$$a(c)\mathbf{u} = -\nabla p, \tag{2.2}$$

$$\phi\frac{\partial c}{\partial t} + \nabla \cdot (\mathbf{u}c) - \nabla \cdot (\mathbf{D}\nabla c) = \tilde{c}q - \phi c z_1 p_t, \tag{2.3}$$

where $a(c) = \frac{\mu(c)}{\kappa(x,y)}$.

Next, we would like to state the following key points, which can be applied to the bound-preserving technique [23].

1. Approximate $r = \phi c$ directly instead of c. Due to the existence of ϕ in (2.3), we cannot obtain the cell averages of c by simply taking the test function to be 1.

2. Treat p_t in (2.3) as a source to apply the positivity-preserving technique.

3. Choose a consistent flux pair (see Definition 2.2.1) for (2.1) and (2.3) to ensure $\bar{r} \leq \bar{\phi}$, where $\bar{r}$ and $\bar{\phi}$ are the cell averages of r and ϕ, respectively.

4. Take the L^2-projection of ϕ into W_h, denoted as Φ, which is the approximation of the porosity.

5. Construct a limiter to maintain the cell average $\bar{r}$ and modify the numerical approximations of r such that $0 \leq r \leq \Phi$, which further yields $c = P_1\left(\frac{r}{\Phi}\right) \in [0, 1]$, where $P_1(u)\,|_K$ is the interpolation of u at the four vertices of cell K.

Unless otherwise stated, we use $p,\ \mathbf{u},\ c$ as the numerical approximations from now on. The IPDG scheme is to find $(p,\ r,\ \mathbf{u}) \in W_h \times W_h \times \mathbf{W}_h$, such that the following variation forms hold for any $(\xi,\ \zeta,\ \boldsymbol{\eta}) \in W_h \times W_h \times \mathbf{W}_h$,

$$(\tilde{d}(r)p_t, \xi) = \mathcal{P}(\mathbf{u}, \xi) + (q, \xi), \tag{2.4}$$

$$(a(c)\mathbf{u}, \boldsymbol{\eta}) = \mathcal{K}(p, \boldsymbol{\eta}), \tag{2.5}$$

$$(r_t, \zeta) = \mathcal{L}^c(\mathbf{u}, c, \zeta) + \mathcal{L}^d(\mathbf{u}, c, \zeta) + (\tilde{c}q - rz_1p_t, \zeta), \tag{2.6}$$

where $c = P_1\left(\frac{r}{\Phi}\right)$, $\tilde{d}(r) = z_1r + z_2(\Phi - r)$, $(u, v) = \int_\Omega uvdxdy$, and

$$\mathcal{P}(\mathbf{u}, \xi) = (\mathbf{u}, \nabla\xi) + \sum_{e\in\Gamma_0} \int_e \hat{\mathbf{u}} \cdot \mathbf{n}_e[\xi]ds, \tag{2.7}$$

$$\mathcal{K}(p, \boldsymbol{\eta}) = (p, \nabla \cdot \boldsymbol{\eta}) + \sum_{e\in\Gamma} \int_e \hat{p}[\boldsymbol{\eta} \cdot \mathbf{n}_e]ds, \tag{2.8}$$

$$\mathcal{L}^c(\mathbf{u}, c, \zeta) = (\mathbf{u}c, \nabla\zeta) + \sum_{e\in\Gamma_0}\int_e \widehat{\mathbf{u}c}\cdot\mathbf{n}_e[\zeta]ds, \tag{2.9}$$

$$\begin{aligned}\mathcal{L}^d(\mathbf{u}, c, \zeta) = &-(\mathbf{D}(\mathbf{u})\nabla c, \nabla\zeta)\\ &-\sum_{e\in\Gamma_0}\int_e (\{\mathbf{D}(\mathbf{u})\nabla c\cdot\mathbf{n_e}\}[\zeta])\,ds\\ &-\sum_{e\in\Gamma_0}\int_e \left(\{\mathbf{D}(\mathbf{u})\nabla\zeta\cdot\mathbf{n_e}\}[c] + \frac{\tilde{\alpha}}{|e|}[c][\zeta]\right)ds.\end{aligned} \tag{2.10}$$

In (2.7)-(2.9), $\hat{p}$, $\hat{\mathbf{u}}$, *and* $\widehat{\mathbf{u}c}$ are the numerical fluxes. We use alternating fluxes for the diffusion terms, and for any $e \in \Gamma_0$

$$\hat{p}|_e = p^-|_e, \quad \hat{\mathbf{u}}|_e = \mathbf{u}^+|_e, \tag{2.11}$$

and on $\partial\Omega$, we take

$$\hat{p}|_e = p^-|_e,\ \forall e \in \partial\Omega_+, \quad \hat{p}|_e = p^+|_e,\ \forall e \in \partial\Omega_-. \tag{2.12}$$

For the convection term, for any $e \in \Gamma_0$, we use

$$\widehat{\mathbf{u}c} = \mathbf{u}^+c^+ - \alpha[c]\mathbf{n}_e, \tag{2.13}$$

where α and $\tilde{\alpha}$ are two positive constants chosen by the bound-preserving technique.

Before we finish this subsection, we would like to introduce the definition of consistent fluxes, which will be used in the bound-preserving technique.

Definition 2.2.1 *$\widehat{\mathbf{u}c}$ and $\hat{\mathbf{u}}$ are said to be consistent if $\widehat{\mathbf{u}c} = \hat{\mathbf{u}}$ by taking $c = 1$ in Ω.*

Obviously, the numerical flux $\widehat{\mathbf{u}c}$ in (2.13) is consistent with $\hat{\mathbf{u}}$ in (2.11), which is required by the bound-preserving technique.

Remark 2.2.1 *There are plenty of consistent fluxes that can be used following the procedures described in Section 2.4. The proofs are basically the same with a few minor changes, so we just list some of them below without further details. We use them in different numerical examples in Section 2.5.*

- $\hat{p} = p^+,\ \hat{\mathbf{u}} = \mathbf{u}^-,\ \widehat{\mathbf{u}c} = \mathbf{u}^- c^- - \alpha[c]\mathbf{n}_e.$

- $\hat{p} = \frac{1}{2}(p^+ + p^-),\ \hat{\mathbf{u}} = \frac{1}{2}(\mathbf{u}^+ + \mathbf{u}^-),\ \widehat{\mathbf{u}c} = \frac{1}{2}(\mathbf{u}^+ c^+ + \mathbf{u}^- c^-) - \alpha[c]\mathbf{n}_e.$

2.3 The SIPEC time integration

In this section, we will develop the SIPEC scheme, which is derived from the SSP-RK2 method with pressure equation solving implicitly and a correction stage. More

generally, we solve the following ordinary differential equations:

$$p_t = f(p, r, q), \tag{2.1}$$

$$r_t = g_1(p, r, b) + g_2(p, r), \tag{2.2}$$

where dependent variables are p and r. q and b are the source terms of the above two equations, respectively. $f(p, r, q)$ corresponds to the right-hand side of the pressure equation. $g_1(p, r, b)$ stands for the convection and the source terms in the concentration equation while $g_2(p, r)$ represents the diffusion term.

Let $\{t^n = n\Delta t\}_{n=0}^{M}$ be a uniform partition of the time interval $[0, T]$ with time step size Δt. We use o^n and $o(t^n)$ $(o = p \; or \; r)$ as the numerical solution and exact solution for (2.1)-(2.2) at time t^n, respectively. For $n = 0$, p^0 and r^0 are L^2-projections of $p(t^0)$ and $r(t^0)$, respectively. When $n \geq 0$, supposing the numerical solutions $p^n,\ r^n$ have been given, we discuss how to find $p^{n+1},\ r^{n+1}$ by the SIPEC method. First, we would obtain $p^{(1)},\ r^{(1)},\ p^{(2)},\ r^{(2)},\ p^{(3)},\ r^{(3)}$ by the following scheme:

$$p^{(1)} = p^n + \Delta t f(p^{(1)}, r^n, q^n), \tag{2.3}$$

$$r^{(1)} = r^n + \Delta t \left(g_1(p^{(1)}, r^n, b^n) + g_2(p^n, r^n) \right), \tag{2.4}$$

$$p^{(2)} = p^{(1)} + \Delta t f(p^{(2)}, r^{(1)}, q^{n+1}), \tag{2.5}$$

$$r^{(2)} = r^{(1)} + \Delta t \left(g_1(p^{(2)}, r^{(1)}, b^{n+1}) + g_2(p^{(1)}, r^{(1)}) \right), \tag{2.6}$$

$$p^{(3)} = \frac{1}{2} p^n + \frac{1}{2} p^{(2)}, \tag{2.7}$$

$$r^{(3)} = \frac{1}{2} r^n + \frac{1}{2} r^{(2)}, \tag{2.8}$$

where $q^{n+1} = q(t^{n+1})$ and $b^{n+1} = b(t^{n+1})$. Notice that (2.1) is solved implicitly while (2.2) is solved explicitly in the above scheme. The scheme is only first-order accurate if we use $p^{(3)}$ and $r^{(3)}$ as the numerical approximations at t^{n+1}. In order to obtain a second-order scheme, we introduce the following correction stage:

$$p^{cor(1)} = p^n + \Delta t f(p^{cor(1)}, r^{(3)}, q^{n+1}), \tag{2.9}$$

$$p^{cor(2)} = p^{(1)} + \Delta t f(p^{cor(2)}, r^{(3)}, q^{n+1}), \tag{2.10}$$

$$\begin{aligned} p^{n+1} &= p^{(3)} - \Delta t \left(f(p^{cor(2)}, r^{(3)}, q^{n+1}) - f(p^{cor(1)}, r^{(3)}, q^{n+1}) \right) \\ &= p^{(3)} + p^{(1)} - p^{cor(2)} + p^{cor(1)} - p^n, \end{aligned} \tag{2.11}$$

$$r^{n+1} = r^{(3)} - \Delta t \left(g_1(p^{cor(2)}, r^{(3)}, b^{n+1}) - g_1(p^{cor(1)}, r^{(3)}, b^{n+1}) \right). \tag{2.12}$$

We call (2.3)-(2.12) the SIPEC scheme. Now, we can state the following theorem.

Theorem 2.3.1 *The SIPEC time integration* (2.3)-(2.8) *and* (2.9)-(2.12) *is second-order accurate in time.*

Proof Follow the local truncation error, we assume $p^n = p(t^n)$ and $r^n = r(t^n)$ are exact solutions at time level n. since (2.3)-(2.8) are derived from the SSP-RK2 method [35], and the standard SSP-RK2 schemes are as follows:

$$\tilde{p}^{(1)} = p^n + \Delta t f(p^n, r^n, q^n), \tag{2.13}$$

$$\tilde{r}^{(1)} = r^n + \Delta t \left(g_1(p^n, r^n, b^n) + g_2(p^n, r^n)\right), \tag{2.14}$$

$$\tilde{p}^{(2)} = \tilde{p}^{(1)} + \Delta t f(\tilde{p}^{(1)}, \tilde{r}^{(1)}, q^{n+1}), \tag{2.15}$$

$$\tilde{r}^{(2)} = \tilde{r}^{(1)} + \Delta t \left(g_1(\tilde{p}^{(1)}, \tilde{r}^{(1)}, b^{n+1}) + g_2(\tilde{p}^{(1)}, \tilde{r}^{(1)})\right), \tag{2.16}$$

$$\tilde{p}^{n+1} = \frac{1}{2}p^n + \frac{1}{2}\tilde{p}^{(2)}, \tag{2.17}$$

$$\tilde{r}^{n+1} = \frac{1}{2}r^n + \frac{1}{2}\tilde{r}^{(2)}. \tag{2.18}$$

Obviously, the above schemes are evaluated explicitly, and after one step we have $\tilde{p}^{n+1} = p(t^{n+1}) + O(\Delta t^3)$, $\tilde{r}^{n+1} = r(t^{n+1}) + O(\Delta t^3)$ as analyzed in [35].

Next, we derive the relationship between (2.3)-(2.8) and (2.13)-(2.18). To be specific,

we can first get

$$p^{(1)} = \tilde{p}^{(1)} - \Delta t f(p^n, r^n, q^n) + \Delta t f(p^{(1)}, r^n, q^n) \tag{2.19}$$

by (2.3) and (2.13). Then, we use (2.5), (2.15) and (2.19) to obtain

$$\begin{aligned} p^{(2)} = \tilde{p}^{(2)} &+ \Delta t \left(f(p^{(2)}, r^{(1)}, q^{n+1}) + f(p^{(1)}, r^n, q^n) \right) \\ &- \Delta t \left(f(p^n, r^n, q^n) + f(\tilde{p}^{(1)}, \tilde{r}^{(1)}, q^{n+1}) \right). \end{aligned} \tag{2.20}$$

Combining (2.7), (2.17) and (2.20), we get

$$\begin{aligned} p^{(3)} &= \tilde{p}^{n+1} + \frac{1}{2}\Delta t \left(f(p^{(2)}, r^{(1)}, q^{n+1}) + f(p^{(1)}, r^n, q^n) \right) \\ &\quad - \frac{1}{2}\Delta t \left(f(p^n, r^n, q^n) + f(\tilde{p}^{(1)}, \tilde{r}^{(1)}, q^{n+1}) \right) \\ &= p(t^{n+1}) + O(\Delta t^3) + \frac{1}{2}\Delta t \left(f(p(t^{n+2}), r(t^{n+1}), q(t^{n+1})) \right) \\ &\quad + \frac{1}{2}\Delta t \left(f(p(t^{n+1}), r(t^n), q(t^n)) \right) \\ &\quad - \frac{1}{2}\Delta t \left(f(p(t^n), r(t^n), q(t^n)) + f(p(t^{n+1}), r(t^{n+1}), q(t^{n+1})) \right). \end{aligned} \tag{2.21}$$

Here we have used the fact that $p^{(2)},\ r^{(1)},\ p^{(1)},\ \tilde{p}^{(1)},\ \tilde{r}^{(1)}$ are second-order approximations of the exact solutions at the corresponding time levels since we only march one step in time. Apply Taylor's expansion, we can obtain

$$f(p(t^{n+2}), r(t^{n+1}), q(t^{n+1})) = f^{n+1} + f_1^{n+1}\Delta t + O(\Delta t^2), \tag{2.22}$$

$$f(p(t^{n+1}), r(t^n), q(t^n)) = f^{n+1} - f_2^{n+1}\Delta t - f_3^{n+1}\Delta t + O(\Delta t^2), \tag{2.23}$$

$$\begin{aligned} f(p(t^n), r(t^n), q(t^n)) &= f^{n+1} - f_1^{n+1}\Delta t \\ &\quad - f_2^{n+1}\Delta t - f_3^{n+1}\Delta t + O(\Delta t^2), \end{aligned} \tag{2.24}$$

where

$$\begin{aligned} f^{n+1} &= f(p(t^{n+1}), r(t^{n+1}), q(t^{n+1})), \\ f_1^{n+1} &= f_1'(p(t^{n+1}), r(t^{n+1}), q(t^{n+1}))p_t(t^{n+1}), \\ f_2^{n+1} &= f_2'(p(t^{n+1}), r(t^{n+1}), q(t^{n+1}))r_t(t^{n+1}), \\ f_3^{n+1} &= f_3'(p(t^{n+1}), r(t^{n+1}), q(t^{n+1}))q_t(t^{n+1}). \end{aligned}$$

Therefore, (2.21) is further transformed into

$$\begin{aligned} &p^{(3)} - \Delta t \left(f(p(t^{n+2}), r(t^{n+1}), q(t^{n+1})) - f(p(t^{n+1}), r(t^{n+1}), q(t^{n+1})) \right) \\ &\quad = p(t^{n+1}) + O(\Delta t^3). \end{aligned} \tag{2.25}$$

Similarly, with direct computation, $r^{(3)}$ can be written as

$$\begin{aligned} & r^{(3)} - \Delta t \left(g_1(p(t^{n+2}), r(t^{n+1}), b(t^{n+1})) - g_1(p(t^{n+1}), r(t^{n+1}), b(t^{n+1})) \right) \\ & = r(t^{n+1}) + O(\Delta t^3). \end{aligned} \tag{2.26}$$

Notice that in (2.26), we do not have the g_2 term, hence it is not necessary to do the correction for the diffusion part.

Moreover, in the correction stage (2.9) and (2.10), it is easy to obtain $p^{cor(1)} = p(t^{n+1}) + O(\Delta t^2)$ and $p^{cor(2)} = p(t^{n+2}) + O(\Delta t^2)$ since we only march one step in time. Therefore, combining (2.11) and (2.25), we have

$$\begin{aligned} p^{n+1} &= p^{(3)} - \Delta t \left(f(p^{cor(2)}, r^{(3)}, q^{n+1}) - f(p^{cor(1)}, r^{(3)}, q^{n+1}) \right) \\ &= p^{(3)} - \Delta t \left(f(p(t^{n+2}), r(t^{n+1}), q(t^{n+1})) \right) \\ &\quad - \Delta t \left(f(p(t^{n+1}), r(t^{n+1}), q(t^{n+1})) \right) + O(\Delta t^3) \\ &= p(t^{n+1}) + O(\Delta t^3). \end{aligned}$$

Similarly, we have $r^{n+1} = r(t^{n+1}) + O(\Delta t^3)$. Therefore, the SIPEC time integration (2.3)-(2.12) is second-order accurate in time. $\square$

Remark 2.3.1 *In* (2.3)-(2.8)*, the variables* p *in diffusion term and convection term are calculated at different time level for two main reasons: (1) To avoid the correction of diffusion term, otherwise it will cause anti-diffusion, and the bound-preserving technique fails to work; (2) In order to preserve the upper bound of* $\bar{r}$*, the fluxes in* (2.1) *and* (2.2) *must be calculated at the same time level. In the correction stage, we use* $r^{(3)}$ *to approximate* $r(t^{n+1})$ *for the sake of the positivity-preserving technique, and* (2.11) *has similar form to* (2.12) *that can preserve upper bound of* $\bar{r}$*, which are all reflected in Section 2.4. Moreover, in* (2.9) *and* (2.10)*, we continue to use implicit scheme to avoid time step size restrictions, which is consistent with* (2.3) *and* (2.5)*.*

Now, we can present the fully-discrete IPDG schemes combined with the SIPEC method. Similar to (2.3)-(2.8), we would get $p^{(1)},\ \mathbf{u}^{(1)},\ r^{(1)},\ p^{(2)},\ \mathbf{u}^{(2)},\ r^{(2)},\ p^{(3)},\ r^{(3)}$ such that for any $\xi,\ \zeta \in W_h$ and $\boldsymbol{\eta} \in \mathbf{W}_h$

$$(\tilde{d}(r^n)p^{(1)}, \xi) = (\tilde{d}(r^n)p^n, \xi) + \Delta t \left(\mathcal{P}(\mathbf{u}^{(1)}, \xi) + (q^n, \xi)\right), \tag{2.27}$$

$$(a(c^n)\mathbf{u}^{(1)}, \boldsymbol{\eta}) = \mathcal{K}(p^{(1)}, \boldsymbol{\eta}), \tag{2.28}$$

$$\begin{aligned}(r^{(1)}, \zeta) = (r^n, \zeta) &+ \Delta t \mathcal{L}^c(\mathbf{u}^{(1)}, c^n, \zeta) \\ &+ \Delta t \left(\mathcal{L}^d(\mathbf{u}^n, c^n, \zeta) + (\tilde{c}^n q^n - r^n z_1 p_t^{(1)}, \zeta)\right),\end{aligned} \tag{2.29}$$

$$(\tilde{d}(r^{(1)})p^{(2)}, \xi) = (\tilde{d}(r^{(1)})p^{(1)}, \xi) + \Delta t \left(\mathcal{P}(\mathbf{u}^{(2)}, \xi) + (q^{n+1}, \xi)\right), \tag{2.30}$$

$$(a(c^{(1)})\mathbf{u}^{(2)}, \boldsymbol{\eta}) = \mathcal{K}(p^{(2)}, \boldsymbol{\eta}), \tag{2.31}$$

$$(r^{(2)},\zeta) = (r^{(1)},\zeta) + \Delta t(\mathcal{L}^c(\mathbf{u}^{(2)},c^{(1)},\zeta) + \mathcal{L}^d(\mathbf{u}^{(1)},c^{(1)},\zeta)$$

$$+(\tilde{c}^{(1)}q^{n+1} - r^{(1)}z_1 p_t^{(2)},\zeta)), \tag{2.32}$$

$$p^{(3)} = \frac{1}{2}p^n + \frac{1}{2}p^{(2)}, \tag{2.33}$$

$$r^{(3)} = \frac{1}{2}r^n + \frac{1}{2}r^{(2)}, \tag{2.34}$$

where $p_t^{(1)} = \frac{p^{(1)}-p^n}{\Delta t}$, $p_t^{(2)} = \frac{p^{(2)}-p^{(1)}}{\Delta t}$, and we use $c = P_1\left(\frac{r}{\Phi}\right)$ to obtain $c^n,\ c^{(1)},\ c^{(2)},\ c^{(3)}$. Then we can find the numerical solutions p^{n+1}, r^{n+1} and $\mathbf{u}^{n+1}$ by the following correction stage

$$(\tilde{d}(r^{(3)})p^{cor(1)},\xi) = (\tilde{d}(r^{(3)})p^n,\xi) + \Delta t\left(\mathcal{P}(\mathbf{u}^{cor(1)},\xi) + (q^{n+1},\xi)\right), \tag{2.35}$$

$$(a(c^{(3)})\mathbf{u}^{cor(1)},\boldsymbol{\eta}) = \mathcal{K}(p^{cor(1)},\boldsymbol{\eta}), \tag{2.36}$$

$$(\tilde{d}(r^{(3)})p^{cor(2)},\xi) = (\tilde{d}(r^{(3)})p^{(1)},\xi) + \Delta t\left(\mathcal{P}(\mathbf{u}^{cor(2)},\xi) + (q^{n+1},\xi)\right), \tag{2.37}$$

$$(a(c^{(3)})\mathbf{u}^{cor(2)},\boldsymbol{\eta}) = \mathcal{K}(p^{cor(2)},\boldsymbol{\eta}), \tag{2.38}$$

$$(\tilde{d}(r^{(3)})p^{n+1},\xi) = (\tilde{d}(r^{(3)})p^{(3)},\xi) - \Delta t\left(\mathcal{P}(\mathbf{u}^{cor(2)},\xi) - \mathcal{P}(\mathbf{u}^{cor(1)},\xi)\right), \tag{2.39}$$

$$(r^{n+1},\zeta) = (r^{(3)},\zeta) - \Delta t\mathcal{L}^c(\mathbf{u}^{cor(2)} - \mathbf{u}^{cor(1)},c^{(3)},\zeta)$$

$$+\Delta t(r^{(3)}z_1(p_t^{cor(2)} - p_t^{cor(1)}),\zeta), \tag{2.40}$$

$$(a(c^{n+1})\mathbf{u}^{n+1},\boldsymbol{\eta}) = \mathcal{K}(p^{n+1},\boldsymbol{\eta}), \tag{2.41}$$

where $p_t^{cor(2)} = \frac{p^{cor(2)}-p^{(1)}}{\Delta t}$ and $p_t^{cor(1)} = \frac{p^{cor(1)}-p^{n}}{\Delta t}$. The flux in (2.40) differs from the previous definition (2.13), i.e. $\widehat{\mathbf{u}^{cor}c^{(3)}} = (\mathbf{u}^{cor})^{+}c^{(3)+} + \alpha[c^{(3)}]\mathbf{n}_e$, $\left(\mathbf{u}^{cor} = \mathbf{u}^{cor(2)} - \mathbf{u}^{cor(1)}\right)$. Moreover, in practical computing, (2.39) actually simplifies to $p^{n+1} = p^{(3)} + p^{(1)} - p^{cor(2)} + p^{cor(1)} - p^{n}$.

2.4 Bound-preserving technique

2.4.1 Second-order bound-preserving

In this subsection, we will apply the SIPEC time discretization and develop the bound-preserving IPDG schemes to obtain physically relevant numerical approximations in $\mathbb{R}^2$. For simplicity, we only discuss the technique for cells away from $\partial\Omega$, while the boundary cells can be analyzed following the same lines with minor changes. We can find a similar analysis for the boundary cells in [23]. We use o_{ij} for the numerical approximation o in cell K_{ij} and the cell average is $\bar{o}_{ij}$. We approximate the integrals in (2.27)-(2.41) by 2-point Gaussian quadratures, and denote $\{x_i^1, x_i^2\}$ and $\{y_j^1, y_j^2\}$ as the Gaussian quadrature points on I_i and J_j, respectively. The corresponding weights on the interval $[-\frac{1}{2}, \frac{1}{2}]$ are represented as w_1 and w_2. Moreover, we define the values of $o(x^+_{i+\frac{1}{2}}, y_j^{\beta})$, $o(x_i^{\beta}, y^+_{j+\frac{1}{2}})$ and $o(x^+_{i+\frac{1}{2}}, y^+_{j+\frac{1}{2}})$ as $o^+_{i+\frac{1}{2},j,\beta}$, $o^+_{i,j+\frac{1}{2},\beta}$and $o^{++}_{i+\frac{1}{2},j+\frac{1}{2}}$, respectively. The same is true for the other values.

In [23], we have completed the bound-preserving analysis for IPDG schemes with forward Euler time integration, which can be directly extended to the bound-preserving analyses of $r^{(1)}$ and $r^{(2)}$ in (2.27)-(2.32). Therefore, we have the following theorem for $r^{(1)}$, and the analysis for $r^{(2)}$ is similar.

Theorem 2.4.1 *Suppose* $0 \le r^n \le \Phi$, *and the parameters* α *and* $\tilde{\alpha}$ *satisfy*

$$\alpha \ge \max_{\substack{2\le i\le N_x-1,\\ 2\le j\le N_y-1,\\ \beta=1,2}} \{{u_1}^{(1)+}_{i+\frac{1}{2},j,\beta},\ {u_2}^{(1)+}_{i,j+\frac{1}{2},\beta},\ 0\}, \tag{2.1}$$

$$\tilde{\alpha} \ge \max\left\{\frac{\Delta y}{2\Delta x}D_{11}^M + \sqrt{3}D_{12}^M,\ \frac{\Delta x}{2\Delta y}D_{22}^M + \sqrt{3}D_{21}^M\right\}, \tag{2.2}$$

where $D_{mn}^M = \max\limits_{(x,y)\in\Omega} |D_{mn}(\mathbf{u}^n)(x,y)|$ $(m,n=1,2)$. *Moreover, if the fluxes* $\widehat{\mathbf{u}c}$ *and* $\widehat{\mathbf{u}}$ *are consistent, then* $0 \le \bar{r}^{(1)} \le \bar{\Phi}$, *under the conditions*

$$\frac{\Delta t}{\Delta x} + \frac{\Delta t}{\Delta y} \le \frac{1}{6}\min\left\{\frac{\Phi_m}{\alpha},\ A_1^{(1)},\ A_2^{(1)}\right\}, \tag{2.3}$$

$$D_{11}^M\frac{\Delta t}{\Delta x^2} + 2(\tilde{\alpha} + D_{12}^M)\frac{\Delta t}{\Delta x\Delta y} \le \frac{1}{12}\Phi_m, \tag{2.4}$$

$$D_{22}^M\frac{\Delta t}{\Delta y^2} + 2(\tilde{\alpha} + D_{21}^M)\frac{\Delta t}{\Delta x\Delta y} \le \frac{1}{12}\Phi_m, \tag{2.5}$$

$$\Delta t \le \frac{1}{6}\min\left\{\frac{1}{z_1 p_M^{(1)}},\ \frac{1}{z_2 p_M^{(1)}},\ \frac{\Phi_m}{q_M}\right\}, \tag{2.6}$$

where

$$\Phi_m = \min_{(x,y)\in\Omega} \Phi(x,y), \quad p_M^{(1)} = \max_{\substack{i,j,\\ \beta,\gamma=1,2}} \left\{ p_t^{(1)}(x_i^\beta, y_j^\gamma),\ 0 \right\}, \quad q_M^n = \max_{\substack{i,j,\\ \beta,\gamma=1,2}} \left\{ -q^n(x_i^\beta, y_j^\gamma),\ 0 \right\},$$

$$A_1^{(1)} = \min_{\substack{2\le i\le N_x-1,\\ 2\le j\le N_y-1,\\ \beta=1,2}} \frac{\Phi^{+\mp}_{i-\frac{1}{2},j\pm\frac{1}{2}}}{\alpha - {u_1}^{(1)+}_{i-\frac{1}{2},j,\beta}}, \quad A_2^{(1)} = \min_{\substack{2\le i\le N_x-1,\\ 2\le j\le N_y-1,\\ \beta=1,2}} \frac{\Phi^{\mp+}_{i\pm\frac{1}{2},j-\frac{1}{2}}}{\alpha - {u_2}^{(1)+}_{i,j-\frac{1}{2},\beta}}.$$

Based on the above theorem, we immediately conclude $0 \le \bar{r}^{(3)} \le \bar{\Phi}$ by (2.34). Next, we demonstrate the bound-preserving technique for $\bar{r}^{n+1}$. In (2.40), take $\zeta = 1$ in K_{ij} to obtain the equation satisfied by $\bar{r}^{n+1}$

$$\bar{r}_{ij}^{n+1} = H^c(r, \mathbf{u}, c) + H^s(r, p_t), \tag{2.7}$$

where

$$\begin{aligned} H^c(r,\mathbf{u},c) = {} & \frac{1}{2}\bar{r}_{ij}^{(3)} \\ & -\lambda\left(\int_{J_j} \widehat{u_1^{cor}c^{(3)}}_{i-\frac{1}{2},j} - \widehat{u_1^{cor}c^{(3)}}_{i+\frac{1}{2},j} dy\right) \\ & -\lambda\left(\int_{I_i} \widehat{u_2^{cor}c^{(3)}}_{i,j-\frac{1}{2}} - \widehat{u_2^{cor}c^{(3)}}_{i,j+\frac{1}{2}} dx\right), \end{aligned} \tag{2.8}$$

$$H^s(r,p_t) = \frac{1}{2}\bar{r}_{ij}^{(3)} + \Delta t z_1 \overline{r_{ij}^{(3)} p_t^{cor}}, \tag{2.9}$$

and

$$\mathbf{u}^{cor} = \mathbf{u}^{cor(2)} - \mathbf{u}^{cor(1)},$$

$$p_t^{cor} = p_t^{cor(2)} - p_t^{cor(1)},$$

with $\lambda = \frac{\Delta t}{\Delta x \Delta y}$ and $\mathbf{u}^{cor} = (u_1^{cor}, u_2^{cor})^T$. We consider the source term H^s first.

Lemma 2.4.1 *Suppose $r^{(3)} > 0$ ($c^{(3)} > 0$), then $H^s(r, p_t) \geq 0$ under the condition*

$$\Delta t \leq \frac{1}{2z_1 p_M^{cor}}, \tag{2.10}$$

where

$$p_M^{cor} = \max_{\substack{i,j,\\ \beta,\gamma=1,2}} \left\{ -p_t^{cor}(x_i^\beta, y_j^\gamma), 0 \right\}. \tag{2.11}$$

Proof The cell averages are approximated by the 2-point Gaussian quadrature, then

$$\begin{aligned} H^s(r, p_t) &:= \frac{1}{2}\bar{r}_{ij}^{(3)} + \Delta t z_1 \overline{r_{ij}^{(3)} p_t^{cor}} \\ &= \frac{1}{2} \sum_{\beta,\gamma=1}^{2} r^{(3)}(x_i^\beta, y_j^\gamma) w_\beta w_\gamma + \Delta t z_1 \sum_{\beta,\gamma=1}^{2} r^{(3)}(x_i^\beta, y_j^\gamma) p_t^{cor}(x_i^\beta, y_j^\gamma) w_\beta w_\gamma \\ &= \sum_{\beta,\gamma=1}^{2} w_\beta w_\gamma r^{(3)}(x_i^\beta, y_j^\gamma) \left(\frac{1}{2} + \Delta t z_1 p_t^{cor}(x_i^\beta, y_j^\gamma) \right). \end{aligned}$$

Therefore, if (2.10) is satisfied, $H^s(r, p_t) \geq 0$. $\square$

Now we analyze the convection term H^c and the lemma is shown below.

Lemma 2.4.2 *Suppose $r^{(3)} > 0$ ($c^{(3)} > 0$), then $H^c(r, \mathbf{u}, c) \geq 0$ if α and the time*

step Δt satisfy

$$\alpha \geq \max_{\substack{2\leq i\leq N_x-1,\\ 2\leq j\leq N_y-1,\\ \beta=1,2}} \{-u_1{}^{cor+}_{i+\frac{1}{2},j,\beta},\ -u_2{}^{cor+}_{i,j+\frac{1}{2},\beta},\ 0\}, \tag{2.12}$$

and

$$\frac{\Delta t}{\Delta x}+\frac{\Delta t}{\Delta y}\leq \frac{1}{4}\min\left\{\frac{\Phi_m}{\alpha},\ A_1^{cor},\ A_2^{cor}\right\}, \tag{2.13}$$

where $\Phi_m=\min\limits_{(x,y)\in\Omega}\Phi(x,y)$, *and*

$$A_1^{cor}=\min_{\substack{2\leq i\leq N_x-1,\\ 2\leq j\leq N_y-1,\\ \beta=1,2}}\frac{\Phi^{+\mp}_{i-\frac{1}{2},j\pm\frac{1}{2}}}{\alpha+u_1{}^{cor+}_{i-\frac{1}{2},j,\beta}},\quad A_2^{cor}=\min_{\substack{2\leq i\leq N_x-1,\\ 2\leq j\leq N_y-1,\\ \beta=1,2}}\frac{\Phi^{\mp+}_{i\pm\frac{1}{2},j-\frac{1}{2}}}{\alpha+u_2{}^{cor+}_{i,j-\frac{1}{2},\beta}}.$$

Proof As the general treatment, we rewrite the cell average $\bar{r}_{ij}^{(3)}$ in the following form:

$$\bar{r}_{ij}^{(3)}=\sum_{\beta=1}^{2}\frac{w_\beta}{2}(r^{(3)+}_{i-\frac{1}{2},j,\beta}+r^{(3)-}_{i+\frac{1}{2},j,\beta})=\sum_{\beta=1}^{2}\frac{w_\beta}{2}(r^{(3)+}_{i,j-\frac{1}{2},\beta}+r^{(3)-}_{i,j+\frac{1}{2},\beta}).$$

Denote $\lambda_1=\frac{\Delta t}{\Delta x}$ and $\lambda_2=\frac{\Delta t}{\Delta y}$, then

$$\begin{aligned}H^c(r,\mathbf{u},c)=&\left(\frac{\lambda_1}{2(\lambda_1+\lambda_2)}\bar{r}_{ij}^{(3)}-\lambda\int_{J_j}\widehat{u_1^{cor}c^{(3)}}_{i-\frac{1}{2},j}-\widehat{u_1^{cor}c^{(3)}}_{i+\frac{1}{2},j}dy\right)\\&+\left(\frac{\lambda_2}{2(\lambda_1+\lambda_2)}\bar{r}_{ij}^{(3)}-\lambda\int_{I_i}\widehat{u_2^{cor}c^{(3)}}_{i,j-\frac{1}{2}}-\widehat{u_2^{cor}c^{(3)}}_{i,j+\frac{1}{2}}dx\right)\\:=&\sum_{\beta=1}^{2}w_\beta\left(\lambda_1L_1+\lambda_2L_2\right),\end{aligned}$$

where

$$L_1 = \frac{1}{4(\lambda_1+\lambda_2)}(r^{(3)+}_{i-\frac{1}{2},j,\beta} + r^{(3)-}_{i+\frac{1}{2},j,\beta}) - (\widehat{u_1^{cor}c^{(3)}})_{i-\frac{1}{2},j,\beta} + (\widehat{u_1^{cor}c^{(3)}})_{i+\frac{1}{2},j,\beta},$$
$$L_2 = \frac{1}{4(\lambda_1+\lambda_2)}(r^{(3)+}_{i,j-\frac{1}{2},\beta} + r^{(3)-}_{i,j+\frac{1}{2},\beta}) - (\widehat{u_2^{cor}c^{(3)}})_{i,j-\frac{1}{2},\beta} + (\widehat{u_2^{cor}c^{(3)}})_{i,j+\frac{1}{2},\beta}.$$

We only need to show $L_1 \geq 0$, and $L_2 \geq 0$. Notice that r and c are both linear functions in I_i and J_j, then it is easy to check that

$$r^{+}_{i-\frac{1}{2},j,\beta} = \mu_1^\beta r^{++}_{i-\frac{1}{2},j-\frac{1}{2}} + \mu_2^\beta r^{+-}_{i-\frac{1}{2},j+\frac{1}{2}} = \mu_1^\beta c^{++}_{i-\frac{1}{2},j-\frac{1}{2}}\Phi^{++}_{i-\frac{1}{2},j-\frac{1}{2}} + \mu_2^\beta c^{+-}_{i-\frac{1}{2},j+\frac{1}{2}}\Phi^{+-}_{i-\frac{1}{2},j+\frac{1}{2}},$$

$$c^{+}_{i-\frac{1}{2},j,\beta} = \mu_1^\beta c^{++}_{i-\frac{1}{2},j-\frac{1}{2}} + \mu_2^\beta c^{+-}_{i-\frac{1}{2},j+\frac{1}{2}},$$

with $\mu_1^1 = \mu_2^2 = \frac{3+\sqrt{3}}{6}$ and $\mu_1^2 = \mu_2^1 = \frac{3-\sqrt{3}}{6}$.

Therefore,

$$\begin{aligned}
L_1 =& c^{(3)++}_{i-\frac{1}{2},j-\frac{1}{2}}\mu_1^\beta\left(\frac{\Phi^{++}_{i-\frac{1}{2},j-\frac{1}{2}}}{4(\lambda_1+\lambda_2)} - u_1{}^{cor+}_{i-\frac{1}{2},j,\beta} - \alpha\right)\\
&+ c^{(3)+-}_{i-\frac{1}{2},j+\frac{1}{2}}\mu_2^\beta\left(\frac{\Phi^{+-}_{i-\frac{1}{2},j+\frac{1}{2}}}{4(\lambda_1+\lambda_2)} - u_1{}^{cor+}_{i-\frac{1}{2},j,\beta} - \alpha\right)\\
&+ c^{(3)-+}_{i+\frac{1}{2},j-\frac{1}{2}}\mu_1^\beta\left(\frac{\Phi^{-+}_{i+\frac{1}{2},j-\frac{1}{2}}}{4(\lambda_1+\lambda_2)} - \alpha\right) + c^{(3)-+}_{i-\frac{1}{2},j-\frac{1}{2}}\mu_1^\beta\alpha\\
&+ c^{(3)--}_{i+\frac{1}{2},j+\frac{1}{2}}\mu_2^\beta\left(\frac{\Phi^{--}_{i+\frac{1}{2},j+\frac{1}{2}}}{4(\lambda_1+\lambda_2)} - \alpha\right) + c^{(3)--}_{i-\frac{1}{2},j+\frac{1}{2}}\mu_2^\beta\alpha\\
&+ c^{(3)++}_{i+\frac{1}{2},j-\frac{1}{2}}\mu_1^\beta\left(u_1{}^{cor+}_{i+\frac{1}{2},j,\beta} + \alpha\right) + c^{(3)+-}_{i+\frac{1}{2},j+\frac{1}{2}}\mu_2^\beta\left(u_1{}^{cor+}_{i+\frac{1}{2},j,\beta} + \alpha\right).
\end{aligned}$$

Then we have $L_1 \geq 0$ if α and $\lambda_1+\lambda_2$ satisfy (2.12) and (2.13), respectively. Similarly, L_2 is transformed in the same way. Then $L_2 \geq 0$ under the conditions (2.12) and (2.13). $\square$

The above lemmas guarantee $\bar{r}^{n+1}$ is positive. However, we still need to prove $\bar{r}^{n+1} \leq \bar{\Phi}$, and the result is as follows.

Theorem 2.4.2 *Suppose the conditions in Lemma 2.4.1 and Lemma 2.4.2 are satisfied. Moreover, we assume* $0 \leq r^{(3)} \leq \Phi$ *and the flux pair* $(\widehat{\mathbf{u}c}, \widehat{\mathbf{u}})$ *is consistent, then* $0 \leq \bar{r}^{n+1} \leq \bar{\Phi}$ *under another condition*

$$\Delta t \leq \frac{1}{2z_2 p_M^{cor}}, \tag{2.14}$$

where p_M^{cor} *is given in* (2.11).

Proof Since the flux pair $(\widehat{\mathbf{u}c}, \widehat{\mathbf{u}})$ are consistent, $\widehat{\mathbf{u}} - \widehat{\mathbf{u}c} = \widehat{\mathbf{u}c_2}$ where $c_2 = 1 - c$. Take $\xi = \zeta$ in (2.39), and subtract (2.40) from (2.39) to obtain

$$(r_2^{n+1}, \zeta) = (r_2^{(3)}, \zeta) - \Delta t \left((\mathbf{u}^{cor} c_2^{(3)}, \nabla\zeta) + \sum_{e \in \Gamma_0} \int_e \widehat{\mathbf{u}^{cor} c_2^{(3)}} \cdot \mathbf{n}_e [\zeta] ds - (r_2^{(3)} z_2 p_t^{cor}, \zeta) \right), \tag{2.15}$$

where $r_2 = \Phi - r$. We can easily check that (2.15) is exactly (2.40) with $r,\ c,$ *and* z_1 replaced by $r_2,\ c_2,$ *and* z_2, respectively. Following the same analyses in Lemma 2.4.1 and Lemma 2.4.2, we can prove $\bar{r}_2^{n+1} \geq 0$ under the conditions given in this theorem,

which further implies $\bar{r}^{n+1} \leq \bar{\Phi}$. $\square$

Remark 2.4.1 *By Theorem 2.4.1 and Theorem 2.4.2, we prove that* $\bar{r}^{(1)}$, $\bar{r}^{(2)}$, $\bar{r}^{(3)}$ *and* $\bar{r}^{n+1}$ *are between* $[0, \bar{\Phi}]$ *under different conditions. In fact, the basic idea of the proofs is the same: first, apply the positivity-preserving techniques to* r*; then, subtract the scheme of the concentration from that of the pressure to obtain that of the second component concentration, and analyze the positivity of* $\bar{r}_2$*; finally, enforce* $r_1 + r_2 = \Phi$ *(*$c_1 + c_2 = 1$*) by choosing consistent numerical fluxes.*

Remark 2.4.2 *In practice,* D *would be very small, and the time step size restriction given in Theorem 2.4.1 and Theorem 2.4.2 are very mild unless the meshes are extremely refined. Actually, in all the numerical experiments, we will choose* $\Delta t \sim \Delta x$*.*

2.4.2 Slope limiter

With Theorem 2.4.1 and Theorem 2.4.2, we can guarantee the numerical cell averages $\bar{r}^{(1)}$, $\bar{r}^{(2)}$, $\bar{r}^{(3)}$, and $\bar{r}^{n+1}$ to be physically relevant. However, the corresponding numerical approximations of r may be negative or larger than Φ. Therefore, we need to apply a slope limiter to modify r. As discussed in [29], the procedure is given in the following steps.

1. Define $\hat{S} = \{(x, y) \in K : \ r(x, y) \leq 0\}$. Take

$$\hat{r} = r + \theta \left(\frac{\bar{r}}{\bar{\Phi}} \Phi - r \right), \quad \theta = \max_{(x,y)\in\hat{S}} \left\{ \frac{-r(x, y)\bar{\Phi}}{\bar{r}\Phi(x, y) - r(x, y)\bar{\Phi}}, \ 0 \right\};$$

2. Set $r_2 = \Phi - \hat{r}$, and repeat the above step for r_2 to get $\hat{r}_2$;

3. Take $\tilde{r} = \Phi - \hat{r}_2$ as the new approximation.

Remark 2.4.3 *After the above three steps, we have* $0 \leq \tilde{r} \leq \Phi$. *It is easy to check that the limiter does not change the numerical cell averages, i.e.* $\int_{K_{ij}} \tilde{r}(x)dx = \int_{K_{ij}} r(x)dx$. *Moreover, it is proved that the limiter does not affect the accuracy. See [29] for more information.*

2.5 Numerical experiments

In this section, we provide numerical examples to illustrate the accuracy and capability of the bound-preserving IPDG method with the SIPEC time discretization for compressible miscible displacements in porous media.

2.5.1 One dimensional case

In this subsection, we solve compressible miscible displacements in one space dimension on the computational domain $[0, 2\pi]$. Unless otherwise stated, we set $N = 80$ and $\Delta x = \frac{2\pi}{N}$. In the first example, we test the accuracy of the fully-discrete SIPEC-IPDG schemes with and without bound-preserving technique.

Example 2.5.1

We set the initial conditions as

$$c(x, 0) = \frac{1}{2}\left(1 - \cos(x)\right), \; p(x, 0) = \cos(x) - 1,$$

and source parameters q and $\tilde{c}$ are taken as

$$q(x, t) = e^{-t}, \; \tilde{c} = \frac{1}{2}\left(e^{-\gamma t}(\sin^2(x) - \cos(x)) + 1\right).$$

Moreover, we choose other parameters as

$$z_1 = z_2 = 1, \; \phi(x) = 1, \; D(u) = \gamma, \; \kappa(x) = \mu(c) = 1.$$

It is easy to verify that the exact solutions are

$$c(x,t) = \frac{1}{2}\left(1 - e^{-\gamma t}\cos(x)\right),\ p(x,t) = e^{-t}\left(\cos(x) - 1\right).$$

In the numerical simulation, we take $\Delta t = 0.16\Delta x$ and final time $T = 1$. We choose $\gamma = 10^{-5}$ such that the exact solution c is very close to 0 for $t > 0$, causing the bound-preserving limiter to be triggered frequently. We compute the L^2-norm of the error between the numerical and exact solutions of c. The results are shown in Table 2.1, where we can observe optimal convergence rates of the SIPEC-IPDG method with and without the bound-preserving limiter. Therefore, the bound-preserving technique

Table 2.1
Example 2.5.1: Accuracy test of c for the fully-discrete SIPEC-IPDG schemes with and without the bound-preserving limiter.

N	With limier		No limiter	
	L^2 error	order	L^2 error	order
10	2.57e-2	-	1.90e-2	-
20	5.57e-3	2.21	4.59e-3	2.05
40	1.26e-3	2.14	1.13e-3	2.02
80	2.98e-4	2.08	2.82e-4	2.01
160	7.21e-5	2.05	7.02e-5	2.00

does not degenerate the accuracy for one dimensional case.

Moreover, we also consider the IMPEC-IPDG method, where the backward and forward Euler methods are used to discretize time derivatives of pressure and concentration, respectively. We also take $\Delta t = 0.16\Delta x$ and $T = 1$, and the results are given

in Table 2.2. From the table, we observe first-order accuracy because of $\Delta t \sim \Delta x$.

Table 2.2
Example 2.5.1: Accuracy test of c for the fully-discrete IMPEC-IPDG schemes with and without the bound-preserving limiter.

N	With limier		No limiter	
	L^2 error	order	L^2 error	order
10	3.22e-2	-	2.89e-2	-
20	1.32e-2	1.29	1.29e-2	1.16
40	6.48e-3	1.03	6.46e-3	1.00
80	3.28e-3	0.98	3.27e-3	0.98
160	1.66e-3	0.98	1.66e-3	0.98

Next, we consider the following example to test the effect of the bound-preserving technique.

Example 2.5.2

We choose the initial conditions as

$$c(x,0) = \frac{1}{2}\left(\cos(x)+1\right),\ p(x,0) = -\gamma\cos(x).$$

Other parameters are taken as

$$q(x,t) = 0,\ z_1 = 0.35,\ z_2 = \mu(c) = \kappa(x) = 1,\ \phi(x) = \frac{1}{4}\left(3+\cos(x)\right),\ D(u) = 0.$$

First, we compute the concentration c at final time $T = 1$ with $\Delta t = 0.02\Delta x$. Since

$D = 0$, the diffusion term cannot provide any stability to the numerical schemes. We set $\gamma = 1,\ 2,\ 3,\ 4$ and apply the bound-preserving limiter. The numerical results of c are given in Figure 2.1. From the figure, we can see that the larger

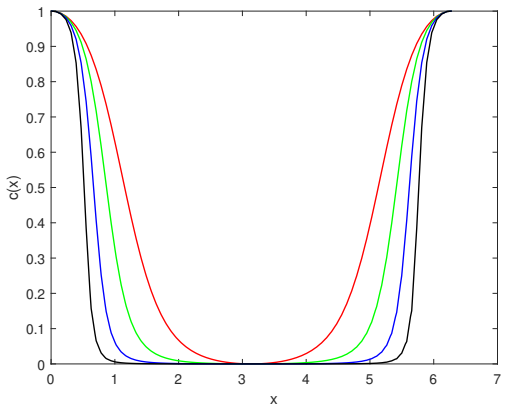

Figure 2.1 Example 2.5.2: Numerical approximations of c for $\gamma = 1$ (red), 2 (green), 3 (blue), 4 (black) with bound-preserving limiter.

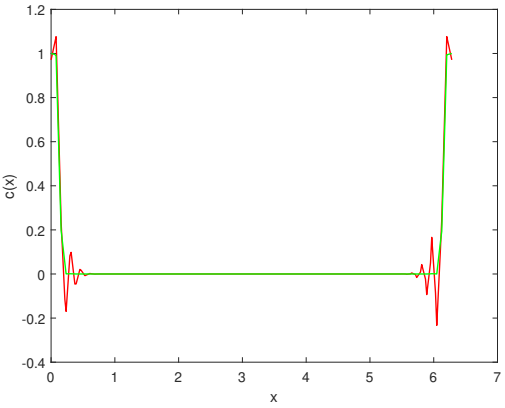

Figure 2.2 Example 2.5.2: Numerical approximations of c for $\gamma = 10$ with (green) and without (red) bound-preserving limiter.

the γ, the larger the gradient of the numerical approximation. We also set $\gamma = 10$ to test the effect of the bound-preserving limiter. The results are shown in Figure 2.2, where the green and red curves are the numerical approximations c obtained

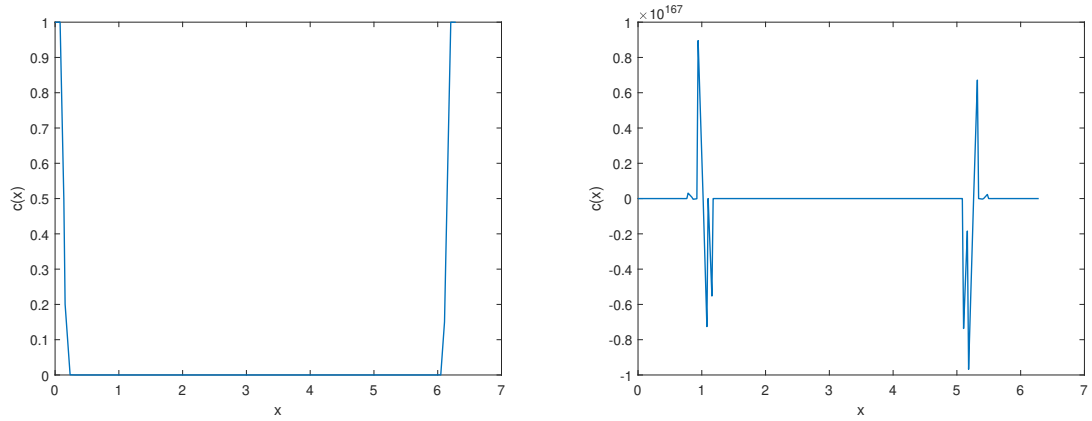

(a) c by SIPEC time discretization (b) c by IMPEC time discretization

Figure 2.3 Example 2.5.2: Concentrations c by different time methods at T=1.

with and without the bound-preserving limiter, respectively. We can observe that, with the bound-preserving limiter, the green curve is not oscillatory and the numerical approximation lies between 0 and 1. This figure clearly demonstrates that the bound-preserving technique is effective, which can avoid strong oscillation and physically irrelevant values.

Next, we change the time step size $\Delta t = 0.08\Delta x$ to test the difference between the SIPEC and the IMPEC methods. The numerical approximations of c are shown in Figure 2.3. It is easy to see that Figure 2.3(b) is clearly unstable. In fact, if the time step size is reduced to $0.07\Delta x$, the result by the IMPEC method is the same as that of Figure 2.3(a), which indicates that the time step size of the SIPEC method can be larger than that of the IMPEC method.

Example 2.5.3

We choose the initial conditions as

$$c(x,0) = \begin{cases} 1, & x < 1, \\ \\ 0, & x \geq 1, \end{cases} \qquad p(x,0) = \begin{cases} 5, & x < 1, \\ \\ 0, & x \geq 1. \end{cases}$$

Other parameters are taken as

$$q(x,t) = 0,\ z_1 = 0.1,\ \kappa(x) = \mu(c) = z_2 = 1,\ \phi(x) = 1,\ D(u) = 0.$$

We compute concentration c at time $T = 1$ with $\Delta t = 0.06\Delta x$. We solve the problem with the bound-preserving limiter, and the result is shown in Figure 2.4. We can observe that the numerical approximation of c is between 0 and 1. Next, we solve the problem without the bound-preserving limiter and the numerical approximation blows up at $T \approx 0.002$ s even though we take time step size as small as $\Delta t = 0.0001\Delta x$. In [23], we proved that the blow-up of the numerical approximation is caused by the ill-posedness of the system. This result demonstrates the necessity of the bound-preserving technique for compressible miscible displacements in porous media.

Moreover, we simulate the example with the SSP-RK2 time discretization. It turns out that the CPU time by the SSP-RK2 method is about 156.5 s with maximum time step size $\Delta t = 0.0004\Delta x$, while the CPU time by the SIPEC method is about 4.3 s with time step size $\Delta t = 0.06\Delta x$. Therefore, we can conclude that the SIPEC

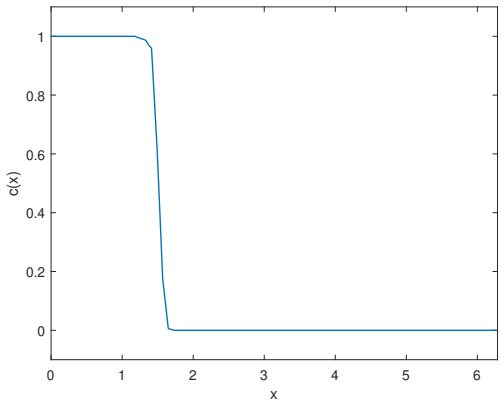

Figure 2.4 Example 2.5.3: Numerical approximations of c at $T = 1$.

method is superior to the traditional SSP-RK2 method.

In addition to the above, we also test the difference between the SIPEC and the IMPEC methods. The results are shown in Figure 2.5, where the red and blue curves are the numerical approximations of c obtained by the SIPEC and the IMPEC method, respectively. We can see that when the time step size is small, the difference between the two methods is tiny. Moreover, the larger the time step size, the more significant the difference. More precisely, the SIPEC method is better than the IMPEC method based on the following three points: (1) The oscillation of c obtained from the SIPEC scheme is less than that from the IMPEC scheme. (2) The time step size has little effect on the SIPEC scheme. (3) The time step size of the SIPEC method can be much larger than that of the IMPEC method.

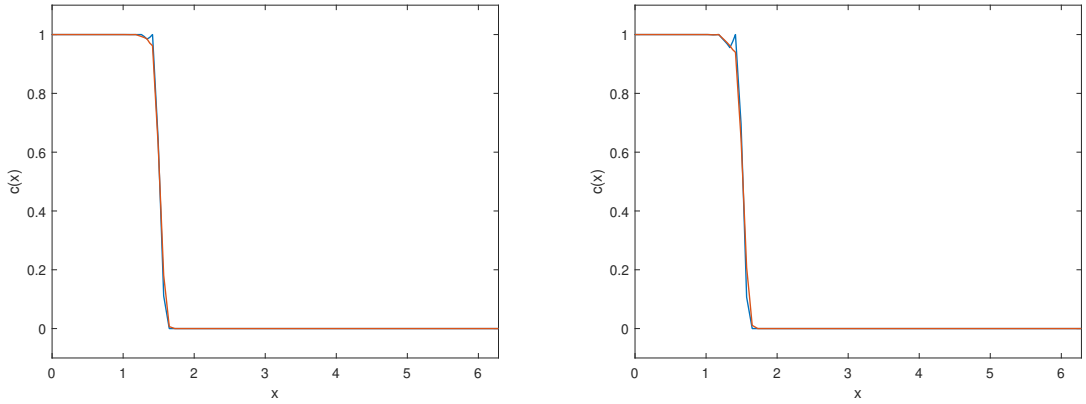

(a) c with $\Delta t = 0.06\Delta x$

(b) c with $\Delta t = 0.12\Delta x$

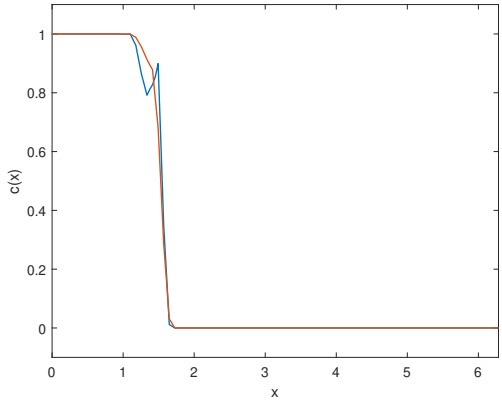

(c) c with $\Delta t = 0.18\Delta x$

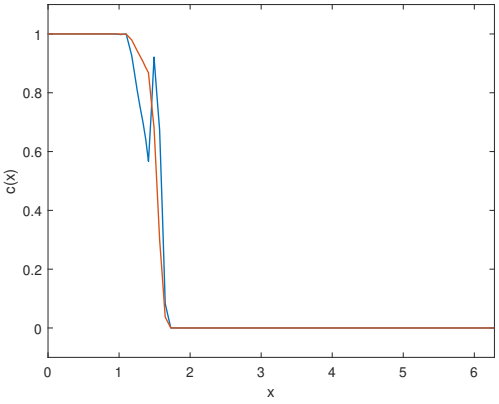

(d) c with $\Delta t = 0.2\Delta x$

Figure 2.5 Example 2.5.3: Concentrations c by SIPEC (red) and IMPEC (blue) time discretizations at $T = 1$ with different time step size Δt.

2.5.2 Two dimensional case

In this subsection, we solve (2.1)-(2.2) with boundary conditions (2.4). The computational domain is set to be $\Omega = [0, 2\pi] \times [0, 2\pi]$.Unless otherwise stated, we take $N_x = N_y = N$, $\Delta x = \frac{2\pi}{N_x}$ and $\Delta y = \frac{2\pi}{N_y}$. In the following example, we test the accuracy of the bound-preserving IPDG schemes with the SIPEC time discretization.

Example 2.5.4

We set the initial conditions as

$$c(x,y,0) = \frac{1}{2}\left(1-\cos(x)\cos(y)\right),\ p(x,y,0) = \cos(x)\cos(y) - 1,$$

and the source parameters q and $\tilde{c}$ are chosen as

$$\begin{aligned} &q(x,y,t) = 2e^{-2t}, \\ &\tilde{c} = \frac{1}{2}\left(e^{-2\gamma t}\left(\frac{1}{2}\sin^2(x)\cos^2(y) + \frac{1}{2}\cos^2(x)\sin^2(y) - \cos(x)\cos(y)\right) + 1\right). \end{aligned}$$

Moreover, we choose other parameters as

$$z_1 = z_2 = 1,\ \phi(x,y) = \kappa(x,y) = \mu(c) = 1,\ \mathbf{D}(\mathbf{u}) = \begin{pmatrix} \gamma & 0 \\ 0 & \gamma \end{pmatrix}.$$

It is easy to see that the exact solutions are

$$c(x,y,t) = \frac{1}{2}\left(1 - e^{-2\gamma t}\cos(x)\cos(y)\right),\ p(x,y,t) = e^{-2t}\left(\cos(x)\cos(y) - 1\right).$$

We choose $\Delta t = 0.08\min\{\Delta x,\ \Delta y\}$, $T = 0.1$ and $\gamma = 10^{-5}$. The computational results are given in Table 2.3, illustrating the L^2 error and convergence orders for c with and without bound-preserving limiter. We can observe second-order accuracy of

the SIPEC-IPDG methods with and without the bound-preserving limiter. Therefore, the limiter does not kill the accuracy for two dimensional case.

Table 2.3
Example 2.5.4: Accuracy test of c for the fully-discrete SIPEC-IPDG schemes with and without the bound-preserving limiter.

N	With limier		No limiter	
	L^2 error	order	L^2 error	order
10	5.24e-2	-	4.34e-2	-
20	1.12e-2	2.22	1.06e-2	2.03
40	2.68e-3	2.07	2.64e-3	2.01
80	6.61e-4	2.02	6.59e-4	2.00
160	1.65e-4	2.00	1.65e-4	2.00

And we also consider the IMPEC-IPDG methods with $\Delta t = 0.08 \min\{\Delta x,\ \Delta y\},\ T = 0.1$. We can find the results in Table 2.4. The accuracy is first-order. By comparing Table 2.3 and Table 2.4, we conclude that the SIPEC method is better than the IMPEC method.

Table 2.4
Example 2.5.4: Accuracy test of c for the fully-discrete IMPEC-IPDG schemes with and without the bound-preserving limiter.

N	With limier		No limiter	
	L^2 error	order	L^2 error	order
10	5.30e-2	-	4.41e-2	-
20	1.26e-2	2.07	1.20e-2	1.87
40	4.14e-3	1.60	4.12e-3	1.55
80	1.78e-3	1.22	1.78e-3	1.21
160	8.62e-4	1.05	8.62e-4	1.05
320	4.30e-4	1.00	4.30e-4	1.00

Example 2.5.5

We choose the initial conditions as

$$c(x,y,0) = \begin{cases} 1, & x \le \dfrac{\pi}{2},\ y \le \dfrac{\pi}{2}, \\ 0, & otherwise, \end{cases} \qquad p(x,y,0) = \cos\left(\frac{x}{2}\right) + \cos\left(\frac{y}{2}\right).$$

Other parameters are taken as

$$q(x,y,t) = 0,\ z_1 = 1,\ z_2 = 10,\ \mu(c) = \kappa(x,y) = \phi(x,y) = 1,\ \mathbf{D}(\mathbf{u}) = 0.$$

We compute c at final time $T = 0.1,\ 1.0,\ 1.4,\ 2.0$ with $N_x = N_y = 80$, $\Delta t = 0.1 \min\{\Delta x, \Delta y\}$ and the bound-preserving limiter. The results are given in Figure 2.6. From the figures, we can see that the numerical approximations are between 0 and 1. To test the effectiveness of the bound-preserving technique for two dimensional case, we simulate the distributions of c at different time $T = 0.1,\ 1.0$ along the diagonal $y = x$ with and without bound-preserving limiter. The results are given in Figure 2.7. From Figure 2.7(b) and Figure 2.7(d), we can observe strong oscillations and physically irrelevant values, while concentrations c in Figure 2.7(a) and Figure 2.7(c) do not, indicating the effectiveness of the bound-preserving technique.

To test the good performance of the SIPEC method for problems in two space dimensions, we simulate the example with the SSP-RK2 method at $T = 1$. Without the bound-preserving technique, the CPU time by the SSP-RK2 method is about 330.6 s

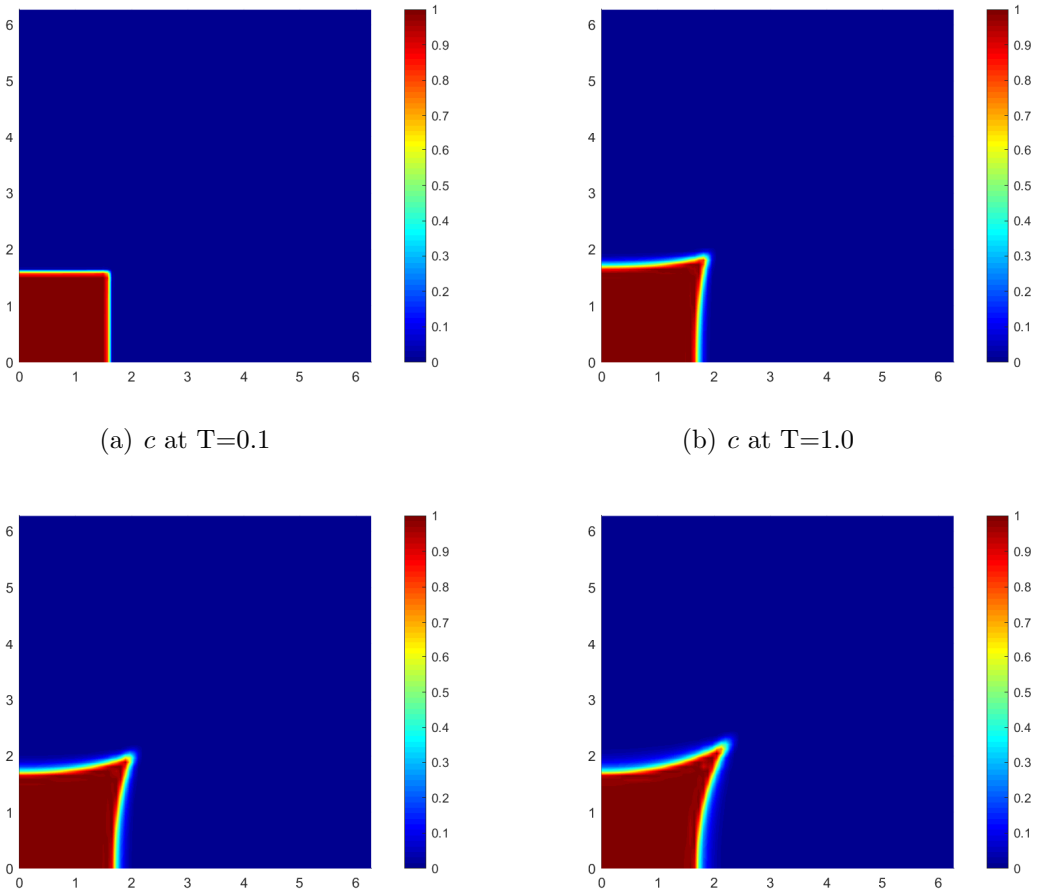

(a) c at T=0.1

(b) c at T=1.0

(c) c at T=1.4

(d) c at T=2.0

Figure 2.6 Example 2.5.5: Concentrations c at different time with bound-preserving limiter.

with maximum time step size $\Delta t = 0.004 \min\{\Delta x, \Delta y\}$, while the CPU time by the SIPEC method is about 45.4 s with time step size $\Delta t = 0.1 \min\{\Delta x, \Delta y\}$. With the bound-preserving technique, the CPU time by the SSP-RK2 method is about 361.1 s with time step size $\Delta t = 0.004 \min\{\Delta x, \Delta y\}$, while the CPU time by the SIPEC method is about 38.4 s with time step size $\Delta t = 0.12 \min\{\Delta x, \Delta y\}$. Through the

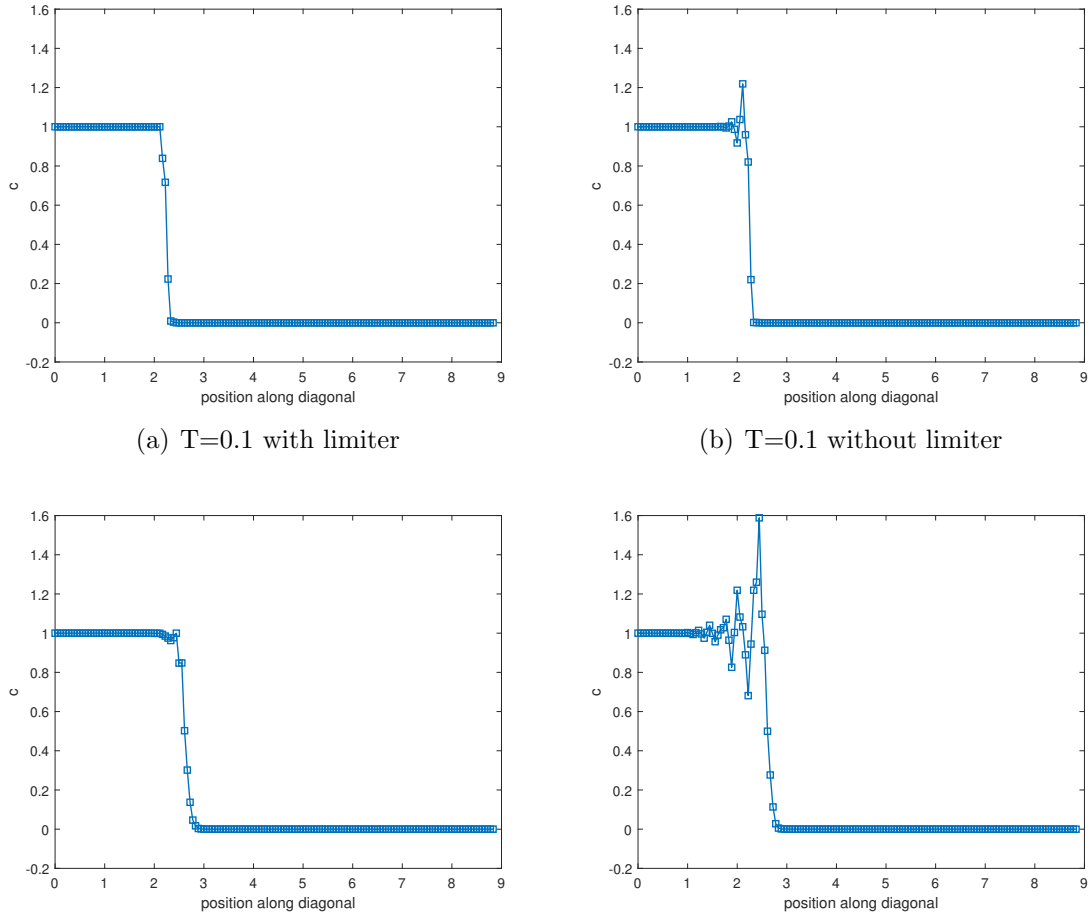

(a) T=0.1 with limiter

(b) T=0.1 without limiter

(c) T=1.0 with limiter

(d) T=1.0 without limiter

Figure 2.7 Example 2.5.5: Concentration c with and without bound-preserving limiter.

above comparison, we can conclude that the SIPEC method is superior to the traditional SSP-RK2 method regardless of whether the bound-preserving technique is used.

Example 2.5.6

We choose the initial conditions as

$$c(x, y, 0) = 0.5,\ p(x, y, 0) = 0.$$

Other parameters are taken as

$$z_1 = 0.4,\ z_2 = 0.6,\ \phi(x, y) = 1,\ \mathbf{D}(\mathbf{u}) = 0.1 \begin{pmatrix} |\mathbf{u}| & 0 \\ 0 & |\mathbf{u}| \end{pmatrix}.$$

The injection well is located at the upper-right corner with $q = \frac{1}{\Delta x \Delta y}$ and $\tilde{c} = 1$, and production well is located at the lower-left corner with $q = -\frac{1}{\Delta x \Delta y}$.

We choose $\Delta t = 0.06 \min\{\Delta x, \Delta y\}$, $N_x = N_y = 40$ and final time $T = 1,\ 5,\ 10,\ 15$. The results are given in Figure 2.8. We can observe that all the numerical approximations of c are between 0 and 1. Therefore, the bound-preserving technique works for the petroleum production simulations.

2.6 Concluding remarks

In this paper, we constructed IPDG methods for two-component compressible miscible displacements in porous media. Bound-preserving technique has been applied to the problems in one and two space dimensions to obtain physically relevant numerical

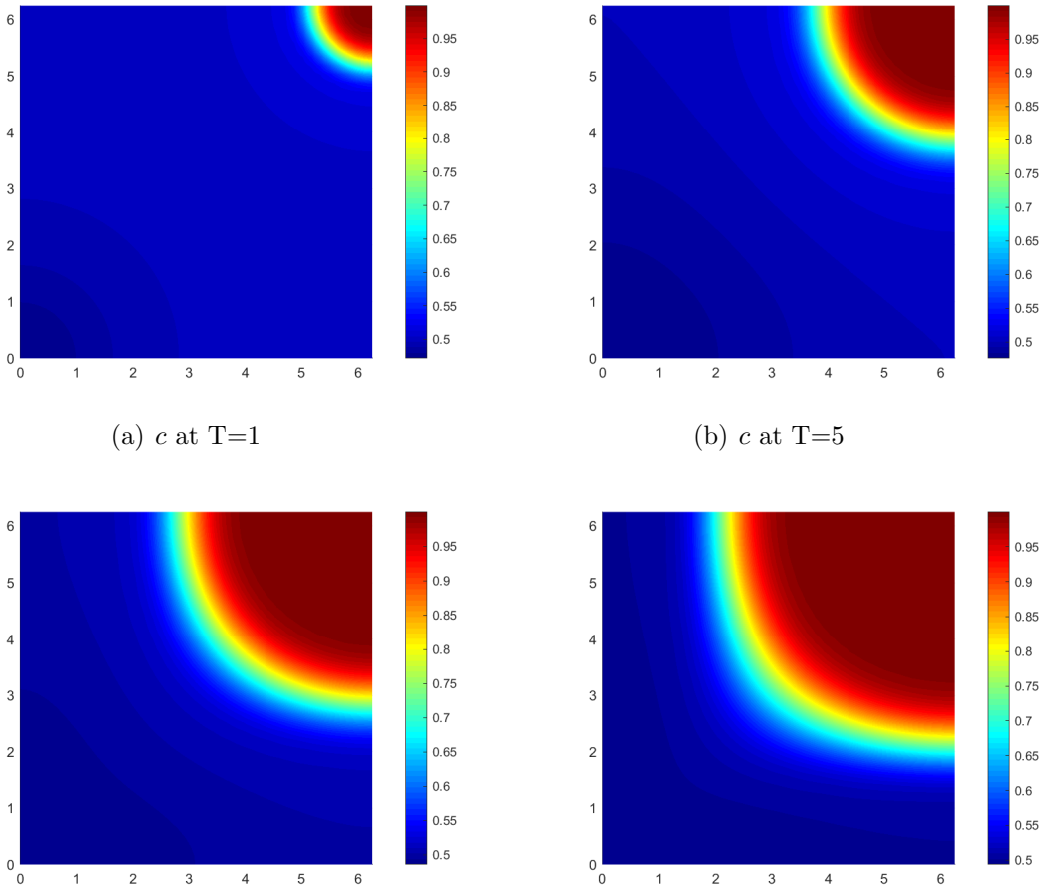

(a) c at T=1

(b) c at T=5

(c) c at T=10

(d) c at T=15

Figure 2.8 Example 2.5.6: Concentration c at different time with bound-preserving limiter.

approximations. Moreover, we presented a novel SIPEC method. Numerical experiments were given to demonstrate the effectiveness of the bound-preserving technique, as well as the superiority of the proposed SIPEC method by comparing it with traditional second-order strong-stability-preserving Runge-Kutta and first-order IMPEC methods. Finally, we point out that the SIPEC method presents a significant advantage compared with the traditional SSP-RK2 if D is small. However, in case D is

large, SIPEC the advantage may not be significant, and we will discuss this in future work.

Chapter 3

Oscillation-free implicit pressure explicit concentration discontinuous Galerkin methods for compressible miscible displacements

The system of compressible miscible displacements is widely adopted to model surfactant flooding in enhanced oil recovery techniques, where a low-viscosity fluid is injected underground to replace the high-viscosity oil. When the mobility ratio of

the injected fluid to oil is high, the waterflood front tends to be unstable and exhibits a finger-like growth pattern, known as viscous fingering. Due to its unstable nature, the viscous fingering phenomenon is sensitive to mesh orientation and numerical discretization. Therefore, high-order numerical methods are preferable to reduce numerical artifacts and mesh dependence. In this paper, we propose a high-order discontinuous Galerkin method for the coupled nonlinear system of compressible miscible displacements to simulate the viscous fingering fluid instability in porous media. We adopt the IMplicit Pressure Explicit Concentration time marching approach based on implicit-explicit Runge-Kutta methods to achieve high-order temporal accuracy. Additionally, we introduce an oscillation-free damping term to control the spurious oscillations encountered in the waterflood front due to the large gradient of saturation. We have conducted ample numerical tests in two space dimensions to demonstrate the effectiveness and robustness of the proposed schemes in recovering viscous fingering.

Keywords: compressible miscible displacements, viscous fingering, discontinuous Galerkin, IMPEC, oscillation-free.

3.1 Introduction

A Hele-Shaw cell consists of two parallel glass plates separated by a narrow space [83]. The distance between the two glass plates is referred to as the width of the

cell's gap. The flow through a Hele-Shaw cell with closely spaced glass plates or a small gap is mathematically analogous to the flow through a two-dimensional porous media[84]. When a less viscous fluid displaces a more viscous one in a porous media, the interface deforms into finger-like patterns, often referred to as viscous fingering [85]. Numerical modeling of viscous fingering dynamics and miscible displacements in porous media holds significant relevance in various applications within oil recovery and addressing environmental pollution. The dynamics of viscous fingering are mathematically modeled using Darcy's law.

The study of miscible displacements in porous media began with their introduction in [1, 2], where mixed finite element methods were utilized. Subsequently, the compressible problem was explored in [3]. Following this, several new numerical methods emerged, including the finite difference method [86], the splitting positive definite mixed element method [5], and the H1-Galerkin mixed method [6]. Additionally, an Eulerian-Lagrangian localized adjoint method was introduced to solve the transport equation, along with a mixed finite element method to solve the flow equation [7]. Furthermore, Kumar [8] developed a mixed and discontinuous finite volume method for incompressible miscible displacement problems. In [9], a discrete duality finite volume scheme was proposed to address the problem, with the convergence of the scheme being studied. In recent years, Discontinuous Galerkin (DG) methods have become increasingly popular for solving compressible miscible displacements in

porous media [10, 11, 12, 13, 14]. Specialized numerical techniques have been developed to manage the jumps in numerical approximations and address the non-linearity of the convection term. Furthermore, extensive research has been conducted on DG methods for incompressible miscible displacements, as evidenced by works such as [8, 15, 16, 18, 19, 67, 87].

Most of the above mentioned methods can effectively simulate most of the problems in miscible displacements. However, if the problem setting is tricky, for example, flow passes an obstacle, the oscillations in the numerical results can be harmful. As demonstrated in [20], direct numerical simulation may result in severe overshoots, leading to nonphysical numerical approximations. The first way to fix this issue is to apply the bound-preserving technique. In the context of convection-diffusion equations, the second-order bound-preserving technique has been explored in [21]. However, extending it to high-order schemes is not a straightforward task. The third-order MPP scheme based on LDG methods on overlapping meshes [24] and direct DG method [25] were introduced. Additionally, other high-order methods have been investigated in [26, 27, 28, 88, 89], which involve modifying numerical fluxes. However, the previous high-order extensions mentioned above have given little attention to bound-preserving techniques for miscible displacements. In many practical scenarios, the physical parameters are closely linked to the concentration c. If c falls outside the interval $[0, 1]$, it is impossible to obtain the parameters in the system. Moreover, in some extreme cases, the numerical approximations may become unstable [23].

We will illustrate this issue through numerical experiments in Section 3.5. In [23], Guo and Yang first proposed bound-preserving DG methods for the coupled system of two-component compressible miscible displacements. The authors theoretically demonstrated in [23] that this algorithm can produce physically relevant numerical cell averages. A slope limiter can then be employed to ensure that the numerical approximations stay within the desired bounds. Later, in [29], the authors expanded this idea to multi-component miscible displacements, proposing high-order bound-preserving DG methods on triangular meshes and showing that the slope limiter does not affect accuracy. Bound-preserving finite difference methods were also developed in [30]. An extension to problems with fractures following this approach can be found in [31].

Unfortunately, the above bound-preserving techniques depend on explicit strong-stability-preserving Runge-Kutta (SSP-RK) time discretizations [34, 35, 36, 37] that require small time step sizes, leading to high computational expenses. As a result, these methods are not viable for numerous applications. The primary factor contributing to the need for small time steps is the heterogeneity of the media, as detailed in [38, 90] and related works. In certain areas of the media, permeability can be exceedingly high, resulting in significant diffusion coefficients in the pressure equation. Hence, an alternative approach involves considering implicit formulations of the pressure equation. Additionally, it is preferable to solve the concentration equation explicitly, as implicit schemes may result in a fully coupled system, leading to

difficulties in implementation. While fully implicit schemes like those in [39, 40] offer unconditional stability, they demand significant computational resources for each time step. In contrast, the IMplicit Pressure Explicit Concentration (IMPEC) scheme [41, 42, 43, 44, 48, 91] has gained popularity for simulating compressible flows in porous media. This scheme involves treating the pressure equation implicitly while updating the concentration equation explicitly. By decoupling the system and solving the equations sequentially, it imposes mild time step size restrictions from the concentration equation. Thus, it is simple to configure, efficient to execute, and requires less computer memory per time step. However, the traditional IMPEC methods are limited to first-order time accuracy, and constructing a second-order IMPEC time method that is compatible with bound-preserving techniques remains challenging. The only work in this direction was given in [50, 51]. Unfortunately, the idea can hardly be used to design a high-order scheme, hence the method cannot effectively simulate viscous fingering phenomena. We will provide comparative tests between the second-order and high-order schemes to demonstrate the necessity of the high order method.

Though the bound-preserving techniques can effectively yield physically relevant numerical approximations, their success depends heavily on theoretical analysis, which is generally not straightforward, especially for high-order methods. Another approach is to effectively suppress the spurious oscillations near the discontinuity in high order DG methods. To do so, various limiters have been developed such as the *minmod*-type

TVD limiter, total variation bounded (TVB) limiter, and weighted ENO (WENO) limiter, etc. For more details, see e.g. [52, 53, 54] and references therein. These limiters aim to adjust the numerical solution post-calculation, utilizing diverse tools and indicators to identify troubled cells, initiating a limiting process for marked cells. However, some limiters are problem-dependent and may compromise the desirable properties of the original schemes. An alternative method involves introducing artificial terms directly into the weak formulation so as to obtain certain properties such as entropy stability or shock capturing, see e.g. [55]. Following this direction, in [56, 92] a damping term was introduced into the DG scheme for hyperbolic equations. Through a unified selection of damping coefficients, the damping term remains small in regions of smooth solutions but becomes effective near the discontinuity. This approach automatically assesses the intensity of the discontinuity, managing numerical oscillations without relying on problem-dependent parameters, and hence easy to implement. In [57], the OFDG methods have been successfully applied to multi-component chemically reacting flows, and the scheme is conservative and bound-preserving. Moreover, numerical experiments demonstrated that the OFDG methods much performs better than the DG schemes with TVD limiters. This motivates us to use OFDG methods to suppress the oscillations and construct the IMPEC methods for miscible displacements.

The aim of the present paper is to propose a new framework to design a conservative high order interior penalty DG scheme with oscillation-free damping term (OFDG)

for the compressible miscible displacements with IMPEC time discretization. The main idea of the IMPEC method is based on the implicit-explicit Runge-Kutta [58] time marching. This treatment can maintain the high-order temporal accuracy while also ensure the large time-step size to save the computational cost. We demonstrate the robustness and accuracy of a fully coupled DG method with an oscillation-free damping term on a rectangular mesh. We provide the simulation of viscous fingering phenomenon by using the high order oscillation-free DG schemes.

The rest of the paper is organized as follows. In Section 3.2, we present the mathematical model that governs the compressible miscible displacement process. In Section 3.3, we introduce the notations to be used throughout the paper then construct the numerical scheme. Later we illustrate high order extension of the proposed scheme in Section 3.4. Then numerical results are given to demonstrate the accuracy and capability of the method in Section 3.5. We end in Section 3.6 with some concluding remarks.

3.2 Mathematical Model

In this section, we present the governing equations that describe the compressible miscible displacements in porous media. Detailed discussion on physical aspects is

provided in [3]. The classical equations governing the compressible miscible displacement in porous media in two spatial dimensions on the computational domain $\Omega = [0, 2\pi] \times [0, 2\pi]$ can be described by the following equations:

$$d(c)\frac{\partial p}{\partial t} + \nabla \cdot \mathbf{u} = q^I - q^P, \quad (x, y) \in \Omega,\ 0 < t \leq T, \tag{3.1}$$

$$\mathbf{u} = -\nabla \cdot \left(\frac{\kappa(x, y)}{\mu(c)} \nabla p \right), \quad (x, y) \in \Omega,\ 0 < t \leq T, \tag{3.2}$$

$$\phi \frac{\partial c}{\partial t} + b(c)\frac{\partial p}{\partial t} + \mathbf{u} \cdot \nabla c - \nabla \cdot (\mathbf{D}\nabla c) = q^I \hat{c} - q^P c, \quad (x, y) \in \Omega,\ 0 < t \leq T \tag{3.3}$$

where the physical unknown variables p, $\mathbf{u}$, and c denote the pressure within the fluid mixture, the Darcy velocity (which measures the volume flowing across a unit cross-section per unit time) of the mixture, and the volumetric concentration of the species of interest, respectively. The flow and transport processes in the system are influenced by the functions q^I and q^P which represent injection wells and production wells respectively. Additionally, the system includes several parameters such as the porosity of the medium, denoted by ϕ, the permeability represented by κ, the fluid viscosity denoted by μ, the injected concentration $\hat{c}$. The dispersion tensor $\mathbf{D}$ can be determined based on a semi-empirical relation [93]

$$\mathbf{D}(\mathbf{u}) = \phi(x, y)(d_{mol}\mathbf{I} + d_{long} |\mathbf{u}| \mathbf{E} + d_{tran} |\mathbf{u}| \mathbf{E}^{\perp}), \tag{3.4}$$

where E is the orthogonal projection along the velocity vector. It takes the form

$$(\mathbf{E}(\mathbf{u}))_{ij} = \frac{u_i u_j}{|\mathbf{u}|^2}, \quad 1 \leq i, j \leq 2, \ \mathbf{u} = (u_1, u_2)^T,$$

and $\mathbf{E}^{\perp} = \mathbf{I} - \mathbf{E}$ is the orthogonal complement. The parameter d_{mol} is related to molecular diffusion; d_{long} measures the longitudinal dispersion, which accounts for dispersion along the direction of flow. and d_{tran} represents the transverse dispersion, which captures dispersion in directions perpendicular to the flow. Here, we assume $\mathbf{D}$ is positive semi-definite. Furthermore, the pressure is uniquely determined except for a constant term. Then we assume $\int_{\Omega} p dx dy = 0$ at $t = 0$. To simplify matters, we focus on a displacement problem involving two components. Extending the analysis to a multi-component fluid is straightforward. The remaining parameters can be described as follows:

$$c_1 = 1 - c_2, \quad d(c) = \phi \sum_{j=1}^{2} z_j c_j, \quad b(c) = \phi c_1 \left\{ z_1 - \sum_{j=1}^{2} z_j c_j \right\},$$

where c_i represents the concentration of the ith component of the fluid mixture, while z_i corresponds to the "constant-compressible" factor. In this paper, we complete the system by impermeable boundary conditions:

$$\mathbf{u} \cdot \mathbf{n} = 0, \quad (\mathbf{D}\nabla c - c\mathbf{u}) \cdot \mathbf{n} = 0, \tag{3.5}$$

where $\mathbf{n}$ represents the unit outer normal of the boundary $\partial\Omega$. The initial solutions of concentration and pressure are provided as follows:

$$c(x, y, 0) = c_0(x, y), \quad p(x, y, 0) = p_0(x, y), \quad (x, y) \in \Omega.$$

3.3 The semi-discrete OFDG scheme

In this section, we will introduce the notations that will be utilized throughout the paper. Subsequently, we will develop the OFDG scheme for the compressible miscible displacement problem (3.1)-(3.3).

3.3.1 Basic notations

We first demonstrate the notation used throughout the paper. We only consider the rectangular meshes in this paper. Let $\Omega = [0, 2\pi]^2$ be the computational domain, comprising of cells

$$K_{i,j} = \{(x, y) : x_{i-\frac{1}{2}} \leq x \leq x_{i+\frac{1}{2}}, y_{j-\frac{1}{2}} \leq y \leq y_{j+\frac{1}{2}}\}, (i = 1, \ldots, N_x,\ j = 1, \ldots, N_y)$$

where $0 = x_{\frac{1}{2}} < \cdots < x_{N_x+\frac{1}{2}} = 2\pi$ and $0 = y_{\frac{1}{2}} < \cdots < y_{N_y+\frac{1}{2}} = 2\pi$ are spatial discretization. The mesh sizes are denoted as $\Delta x_i = x_{i+\frac{1}{2}} - x_{i-\frac{1}{2}}, 1 \le i \le N_x$ and $\Delta y_j = y_{j+\frac{1}{2}} - y_{j-\frac{1}{2}}, 1 \le j \le N_y$, and let $h = \max\left(\max_{1\le i\le N_x} \Delta x_i, \max_{1\le j\le N_y} \Delta y_j\right)$. We assume $K_{i,j} \in \Omega_h$ is a quasi-uniform partition of Ω with rectangular element K, we denote Γ_h as the set of all element interfaces, while $\Gamma_0 = \Gamma_h \backslash \partial\Omega$. For any $e \in \Gamma_h$, $|e|$ represents the length of the edge e. With respect to this mesh, we define the discontinuous finite element space as:

$$W_h^k := \left\{ v \in L^2(\Omega) : v|_{K_{i,j}} \in \mathcal{Q}^k(K_{i,j}), \forall K_{i,j} \in \Omega_h, i \in N_x, y \in N_y \right\},$$

where $\mathcal{Q}_k(K)$=$\mathcal{P}_k(I_i) \otimes \mathcal{P}_k(J_j)$ is the tensor product of two polynomial spaces, $\mathcal{P}_k(K)$ denotes the piecewise polynomials of degree less than or equal to k in K. We choose $\boldsymbol{\beta} = (1, 1)$. Let $\mathbf{n}_e$ be the unit normal vector of $e \in \Gamma_0$, which is the interior edge shared by left elements K_ℓ and right elements K_r, with $\boldsymbol{\beta} \cdot \mathbf{n}_\ell > 0$ and $\boldsymbol{\beta} \cdot \mathbf{n}_r < 0$, where $\mathbf{n}_\ell$ and $\mathbf{n}_r$ are the unit outer normal corresponding to K_ℓ and K_r. Moreover, we denote $\partial\Omega_+ = \{e \in \partial\Omega : \boldsymbol{\beta} \cdot \mathbf{n} > 0\}$, with $\mathbf{n}$ as the unit outer normal of $\partial\Omega$, and $\partial\Omega_- = \partial\Omega \backslash \partial\Omega_+$. Denote $v^+ = (v|_{K_\ell})|_e$ and $v^- = (v|_{K_r})|_e$ as two traces for the functions along edge e and we denote the jump as $[v] = v^+ - v^-$ and $\{v\} = \frac{1}{2}(v^+ + v^-)$ as average of v at the cell interfaces. For the sake of simplicity, for any $e \in \partial\Omega_-$, we define $v^-|_e = 0$,for any $e \in \partial\Omega_+$, we define $v^+|_e = 0$.

3.3.2 The semi-discrete OFDG scheme

To construct the OFDG scheme, we rewrite the coupled system (3.1)-(3.3) into the conservative form:

$$d(c)\frac{\partial p}{\partial t} + \nabla \cdot \mathbf{u} = q, \tag{3.1}$$

$$a(c)\mathbf{u} = -\nabla p, \tag{3.2}$$

$$\phi\frac{\partial c}{\partial t} + \nabla \cdot (\mathbf{u}c) - \nabla \cdot (\mathbf{D}\nabla c) = \tilde{c}q - \phi c z_1 p_t, \tag{3.3}$$

where $a(c) = \frac{\mu(c)}{\kappa(x,y)}$, q as the external volumetric flow rate. We will use $r = \phi c$ instead of c. Denote $p,\ \mathbf{u},\ c$ as the numerical approximations. The OFDG scheme is to find $(p,\ r,\ \mathbf{u}) \in W_h^k \times W_h^k \times \mathbf{W}_h^k$, such that the following variation forms hold for any $(\xi,\ \zeta,\ \boldsymbol{\eta}) \in W_h^k \times W_h^k \times \mathbf{W}_h^k$,

$$(\tilde{d}(r)p_t, \xi) = \mathcal{P}(\mathbf{u}, \xi) + (q, \xi), \tag{3.4}$$

$$(a(c)\mathbf{u}, \boldsymbol{\eta}) = \mathcal{K}(p, \boldsymbol{\eta}), \tag{3.5}$$

$$(r_t, \zeta) = \mathcal{L}^c(\mathbf{u}, c, \zeta) + \mathcal{L}^d(\mathbf{u}, c, \zeta) + \mathcal{L}^{OF}(c, \zeta) + (\tilde{c}q - r z_1 p_t, \zeta), \tag{3.6}$$

where $c = P_1\left(\frac{r}{\Phi}\right)$, $\tilde{d}(r) = z_1 r + z_2(\Phi - r)$, $(u, v) = \int_\Omega uv dx dy$, and

$$\mathcal{P}(\mathbf{u}, \xi) = (\mathbf{u}, \nabla\xi) + \sum_{e\in\Gamma_0} \int_e \hat{\mathbf{u}} \cdot \mathbf{n}_e[\xi] ds, \tag{3.7}$$

$$\mathcal{K}(p, \boldsymbol{\eta}) = (p, \nabla \cdot \boldsymbol{\eta}) + \sum_{e\in\Gamma} \int_e \hat{p}[\boldsymbol{\eta} \cdot \mathbf{n}_e] ds, \tag{3.8}$$

$$\mathcal{L}^c(\mathbf{u}, c, \zeta) = (\mathbf{u}c, \nabla\zeta) + \sum_{e\in\Gamma_0} \int_e \widehat{\mathbf{u}c} \cdot \mathbf{n}_e[\zeta] ds, \tag{3.9}$$

$$\begin{aligned}\mathcal{L}^d(\mathbf{u}, c, \zeta) = &-(\mathbf{D}(\mathbf{u})\nabla c, \nabla\zeta) \\ &- \sum_{e\in\Gamma_0} \int_e \{\mathbf{D}(\mathbf{u})\nabla c \cdot \mathbf{n_e}\}[\zeta] ds \\ &- \sum_{e\in\Gamma_0} \int_e \left(\{\mathbf{D}(\mathbf{u})\nabla\zeta \cdot \mathbf{n_e}\}[c] + \frac{\tilde{\alpha}}{|e|}[c][\zeta] \right) ds,\end{aligned} \tag{3.10}$$

$$\mathcal{L}^{OF}(c, \zeta) = -\sum_{\ell=0}^{k} \frac{\sigma^\ell_{K_{i,j}}(c)}{h_{K_{i,j}}} \int_{K_{i,j}} \left(c - P_h^{\ell-1} c\right) \zeta dx, \tag{3.11}$$

In (2.7)-(2.9), $\hat{p}$, $\hat{\mathbf{u}}$, *and* $\widehat{\mathbf{u}c}$ are the numerical fluxes on the element interfaces. For the diffusion terms, for any $e \in \Gamma_0$,we use alternating fluxes,

$$\hat{p}|_e = p^-|_e, \quad \hat{\mathbf{u}}|_e = \mathbf{u}^+|_e, \tag{3.12}$$

and on $\partial\Omega$, we use

$$\hat{p}|_e = p^-|_e, \ \forall e \in \partial\Omega_+, \quad \hat{p}|_e = p^+|_e, \ \forall e \in \partial\Omega_-. \tag{3.13}$$

For the convection term, for any $e \in \Gamma_0$, we take the Lax-Friedriches flux as follow

$$\widehat{\mathbf{u}c} = \frac{1}{2}(\mathbf{u}^+ c^+ + \mathbf{u}^- c^-) - \alpha[c]\mathbf{n}_e, \tag{3.14}$$

where α and $\tilde{\alpha}$ are two positive constants and called internal penalty.

In oscillation-free damping term (3.11), $P_h^{\ell-1}$ is the standard L_2 projection into $W_h^{\ell-1}, l \geq 0$, that is for any function w, $P_h^\ell w \in W_h^\ell$ satisfies

$$\int_{K_{i,j}} \left(P_h^l w - w\right) v_h dx = 0 \quad \forall v_h \in Q^l\left(K_{i,j}\right). \tag{3.15}$$

We also define $P_h^{-1} = P_h^0$. $\sigma_{K_{i,j}}^\ell$ needs to be chosen carefully since they are small in a smooth region and will be large near discontinuities. In this paper, they are given as follows:

$$\sigma_{K_{i,j}}^\ell(c) = \frac{2(2\ell+1)}{(2k-1)} \frac{h^\ell}{\ell!} \sum_{|\boldsymbol{\alpha}|=\ell} \left(\frac{1}{N_e} \sum_{\boldsymbol{v} \in K_{i,j}} \left([\partial^{\boldsymbol{\alpha}} c]|_{\boldsymbol{v}}\right)^2 \right)^{\frac{1}{2}}. \tag{3.16}$$

Here we only consider the jump of c on the vertex $\boldsymbol{v}$ of two adjacent cells which are shared with edge. N_e is number of vertices of $K_{i,j}$. The vector $\boldsymbol{\alpha} = (\alpha_1, \ldots, \alpha_d)$ is the multi-index of order

$$|\boldsymbol{\alpha}| = \alpha_1 + \cdots + \alpha_d,$$

and $\partial^{\boldsymbol{\alpha}} w$ is defined as

$$\partial^{\boldsymbol{\alpha}} w = \frac{\partial^{|\boldsymbol{\alpha}|} w}{\partial x_1^{\alpha_1} \cdots \partial x_d^{\alpha_d}} = \partial_{x_1}^{\alpha_1} \cdots \partial_{x_d}^{\alpha_d} w.$$

$[w]|_{\boldsymbol{v}}$ denotes the jump of the function w on the vertex $\boldsymbol{v}$ and we can exclusively calculate the jump between element e and its adjoining neighbors. For more details, see [56].

3.4 The IMPEC time integration

In this section, we will discretize in time using IMPEC methods based on the implicit-explicit Runge-Kutta(IMEX-RK) time discretization approach in [58]. First, we introduce the IMEX-RK formulation: An s-stage IMEX-RK scheme can be represented by the following double Butcher tableau:

$$\begin{array}{c|c} \tilde{c} & \tilde{A} \\ \hline & \tilde{b}^T \end{array} \qquad \begin{array}{c|c} c & A \\ \hline & b^T \end{array} \tag{3.1}$$

where $\tilde{A}, A \in \mathbb{R}^{s\times s}, \tilde{c}, c, \tilde{b}, b \in \mathbb{R}^s$. Matrix $\tilde{A} = (\tilde{a}_{ij})$ represents an lower triangular explicit matrix with zero elements on the main diagonal. Matrix $A = (a_{ij})$ is diagonally implicit matrices with $a_{ij} = 0$, for $j > i$. Then we consider the ordinary differential equations as follow:

$$p_t = f(p, r), \tag{3.2}$$

$$r_t = g(p, r, p_t), \tag{3.3}$$

where the dependent variables are p and r. $f(p, r)$ represents the right-hand side of the pressure equation. $g(p, r, p_t)$ corresponds to that in the concentration equation. They can be written as

$$f(p, r) = d^{-1}(r)(\nabla \cdot (a^{-1}(r)\nabla p) + q), \tag{3.4}$$

$$g(p, r, p_t) = -\nabla \cdot (uc) + \nabla \cdot (D(u)\nabla c) + \tilde{c}q - rz_1 p_t. \tag{3.5}$$

We explicitly treat r (using subscript "E") and implicitly treat p (using subscript "I"). The algorithm from time level n to time level $n + 1$ is given as: For $i = 1$ to s

• Compute the internal stages:

$$\begin{aligned} r_E^{(i)} = r^n + \Delta t \tilde{a}_{ij} \sum_{j=1}^{i-1} \left(-\nabla \cdot (u_I^{(j)} c_E^{(j)}) - \nabla \cdot (D(u_I^j)\nabla c_E^{(j)}) \right) \\ + \tilde{a}_{ij} \sum_{j=1}^{i-1} \left(\tilde{c}_E^{(j)} q_I^{(j)} - r_I^j z_1 p_t^{(j)} \right), \end{aligned} \tag{3.6}$$

$$p_*^{(i)} = p_n + \Delta t a_{i,j} \sum_{j=1}^{i-1} \left(d^{-1}(r_E^{(j)})(\nabla \cdot (a^{-1}(c_E^{(j)})\nabla p_I^{(j)}) + q_I^{(j)}) \right), \tag{3.7}$$

$$p^{(i)} = p_*^{(i)} + \Delta t a_{i,i} \left(d^{-1}(r_E^{(i)})(\nabla \cdot (a^{-1}(c_E^{(i)})\nabla p_I^{(i)}) + q_I^{(i)}) \right). \tag{3.8}$$

• Update the numerical solution:

$$p^{n+1} = p^n + \Delta t \sum_{i=1}^{s} b_i \left[d^{-1}(r_E)(\nabla \cdot (a^{-1}(r_E)\nabla p_I) + q_I) \right], \tag{3.9}$$

$$\begin{aligned} r^{n+1} = r^n &+ \Delta t \sum_{i=1}^{s} \tilde{b}_i \left[-\nabla \cdot (u_I c_E) - \nabla \cdot (D(u_I)\nabla c_E) \right] \\ &+ \Delta t \sum_{i=1}^{s} \tilde{b}_i \left(\tilde{c_E} q_I - r_I z_1 p_t \right). \end{aligned} \tag{3.10}$$

Here, we provide more detailed and simplified steps as follows by applying the three-stage IMPEC2 scheme given below to ODE system(3.2)-(3.3)

$$\begin{array}{c|ccc} \tilde{c}_1 & 0 & 0 & 0 \\ \tilde{c}_2 & \tilde{a}_{21} & 0 & 0 \\ \tilde{c}_3 & \tilde{a}_{31} & \tilde{a}_{32} & 0 \\ \hline & \tilde{b}_1 & \tilde{b}_2 & \tilde{b}_3 \end{array} \qquad \begin{array}{c|ccc} c_1 & a_{11} & 0 & 0 \\ c_2 & a_{21} & a_{22} & 0 \\ c_3 & a_{31} & a_{32} & a_{33} \\ \hline & b_1 & b_2 & b_3 \end{array}$$

The five-stage IMPEC3 scheme is straightforward can be obtained following the same

lines.

$$r_E^{(1)} = r^n \tag{3.11}$$

$$p_*^{(1)} = p^n \tag{3.12}$$

$$p_I^{(1)} = p_*^{(1)} + \Delta t a_{11} f(p_I^{(1)}, r_E^{(1)}) \tag{3.13}$$

$$p_t^{(1)} = f(p_I^{(1)}, r_E^{(1)}) \tag{3.14}$$

$$r_E^{(2)} = r^n + \Delta t \tilde{a}_{21} g(p_I^{(1)}, r_E^{(1)}, p_t^{(1)}) \tag{3.15}$$

$$p_*^{(2)} = p^n + \Delta t a_{21} p_t^{(1)} \tag{3.16}$$

$$p_I^{(2)} = p_*^{(2)} + \Delta t a_{22} f(p_I^{(2)}, r_E^{(2)}) \tag{3.17}$$

$$p_t^{(2)} = f(p_I^{(2)}, r_E^{(2)}) \tag{3.18}$$

$$r_E^{(3)} = c^n + \Delta t \tilde{a}_{31} g(p_I^{(1)}, r_E^{(1)}, p_t^{(1)}) + \Delta t \tilde{a}_{32} g(p_I^{(2)}, r_E^{(2)}, p_t^{(2)}) \tag{3.19}$$

$$p_*^{(3)} = p^n + \Delta t a_{31} p_t^{(1)} + \Delta t a_{32} p_t^{(2)} \tag{3.20}$$

$$p_I^{(3)} = p_*^{(3)} + \Delta t a_{33} f(p_I^{(3)}, r_E^{(3)}) \tag{3.21}$$

$$p_t^{(3)} = f(p_I^{(3)}, r_E^{(3)}) \tag{3.22}$$

$$r^{n+1} = r^{(n)} + \Delta t \sum_{i=1}^{s} \tilde{b}_i g(p_I^{(i)}, r_E^{(i)}, p_t^{(i)}) \tag{3.23}$$

$$p^{n+1} = p^{(n)} + \Delta t \sum_{i=1}^{s} b_i p_t^{(i)} \tag{3.24}$$

where p^n, r^n are numerical approximations of $p(t^n)$ and $r(t^n)$ with time step-size Δt

for $n = 0, 1, \cdots, N_T$. Then we can compute $p^{n+1} = p(t^{n+1}), r^{n+1} = r(t^{n+1})$ by the IMPEC2 scheme. The scheme is second-order accurate and we can obtain the third-order accuracy by IMPEC3 scheme. In this paper, we mainly use second and third order Butcher tableaux for IMPEC time marching as follows:

• GSA DIRK(2,2,2) [94]

$$\begin{array}{c|ccc} 0 & 0 & 0 & 0 \\ \gamma & \gamma & 0 & 0 \\ 1 & \delta & 1-\delta & 0 \\ \hline & \delta & 1-\delta & 0 \end{array} \qquad \begin{array}{c|ccc} 0 & 0 & 0 & 0 \\ \gamma & 0 & \gamma & 0 \\ 1 & 0 & 1-\gamma & \gamma \\ \hline & 0 & 1-\gamma & \gamma \end{array} \tag{3.25}$$

where $\gamma = 1 - \frac{\sqrt{2}}{2}$ and $\delta = 1 - \frac{1}{2\gamma}$ with order $p = 2$.

• GSA DIRK(4,4,3) [94]

$$\begin{array}{c|ccccc} 0 & 0 & 0 & 0 & 0 & 0 \\ 1/2 & 1/2 & 0 & 0 & 0 & 0 \\ 2/3 & 11/18 & 1/18 & 0 & 0 & 0 \\ 1/2 & 5/6 & -5/6 & 1/2 & 0 & 0 \\ 1 & 1/4 & 7/4 & 3/4 & -7/4 & 0 \\ \hline & 1/4 & 7/4 & 3/4 & -7/4 & 0 \end{array} \qquad \begin{array}{c|ccccc} 0 & 0 & 0 & 0 & 0 & 0 \\ 1/2 & 0 & 1/2 & 0 & 0 & 0 \\ 2/3 & 0 & 1/6 & 1/2 & 0 & 0 \\ 1/2 & 0 & -1/2 & 1/2 & 1/2 & 0 \\ 1 & 0 & 3/2 & -3/2 & 1/2 & 1/2 \\ \hline & 0 & 3/2 & -3/2 & 1/2 & 1/2 \end{array} \tag{3.26}$$

This method has order $p = 3$.

3.5 Numerical experiments

In this section, we provide numerical tests with IPDG-IMPEC scheme with oscillation-free damping term in two space dimensions to illustrate their accuracy and performance for compressible miscible displacements in porous media. We solve (2.1)-(3.3) with impermeable boundary conditions (2.4). The computational domain is chosen as $\Omega = [0, 2\pi] \times [0, 2\pi]$. Unless otherwise stated, we take $N_x = N_y = 80$, $\Delta x = \frac{2\pi}{N_x}$ and $\Delta y = \frac{2\pi}{N_y}$. We also provide the simulation of viscous fingering phenomenon with some perturbation in the permeability.

Example 3.5.1

We first verify the order of convergence of the two IMPEC approaches by the following coupled ODE system,

$$p_t = 4p - 10r,$$

$$r_t = 4p - p_t - 6r - 10e^{-t}\sin(5t) - 2e^{-2t}\cos(5t)(\cos(5t) + \sin(5t)) + rp.$$

The corresponding exact solutions are

$$p(t) = 2e^{-t}\cos(5t), r(t) = e^{-t}(\cos(5t) + \sin(5t)).$$

We choose the initial time at $t = 0$ and the final time at $t = 1$. The computational results are listed in Table 3.1 and Table 3.2. We can observe the second-order accuracy of the IMPEC2 by using Butcher tableaux (3.25) and the third-order accuracy of IMPEC3 by using Butcher tableaux (3.26).

Table 3.1
Example 3.5.1: Convergence test of p and r for the ODE system with Butcher tableaux (3.25).

Δt	p		r	
	L^2 error	order	L^2 error	order
2^{-6}	6.13e-2	-	3.46e-2	-
2^{-7}	1.48e-2	2.08	8.34e-2	2.78
2^{-8}	3.60e-3	2.05	2.06e-3	2.70
2^{-9}	8.99e-4	2.04	5.15e-4	2.57
2^{-10}	2.24e-4	2.00	1.29e-4	2.40

Table 3.2
Example 3.5.1: Convergence test of p and r for the ODE system with Butcher tableaux (3.26).

Δt	p		r	
	L^2 error	order	L^2 error	order
2^{-6}	2.20e-3	-	3.46e-4	-
2^{-7}	2.84e-4	2.95	8.34e-5	2.96
2^{-8}	3.58e-5	2.99	2.06e-6	2.98
2^{-9}	4.50e-6	2.99	5.15e-7	2.99
2^{-10}	5.65e-7	3.00	1.29e-8	3.00

Example 3.5.2

We now verify orders of accuracy of the system (2.1)-(2.3) in the 2D case. We take the initial data as:

$$c(x, y, 0) = \frac{1}{2}\left(1 - \cos(x)\cos(y)\right), \; p(x, y, 0) = \cos(x)\cos(y) - 1,$$

and choose the source parameters q and $\tilde{c}$ as

$$q(x,y,t) = 2e^{-2t},$$
$$\tilde{c} = \frac{1}{2}\left(e^{-2\gamma t}\left(\frac{1}{2}\sin^2(x)\cos^2(y) + \frac{1}{2}\cos^2(x)\sin^2(y) - \cos(x)\cos(y)\right) + 1\right).$$

Moreover, we take other parameters as

$$z_1 = z_2 = 1,\ \phi(x,y) = \kappa(x,y) = \mu(c) = 1,\ \mathbf{D}(\mathbf{u}) = \begin{pmatrix} \gamma & 0 \\ 0 & \gamma \end{pmatrix}.$$

The corresponding exact solutions are

$$c(x,y,t) = \frac{1}{2}\left(1 - e^{-2\gamma t}\cos(x)\cos(y)\right),\ p(x,y,t) = e^{-2t}\left(\cos(x)\cos(y) - 1\right).$$

We choose $\Delta t = 0.04\min\{\Delta x,\ \Delta y\}$, $T = 0.1$ and $\gamma = 10^{-5}$. The computational results are listed in Table 3.3 and Table 3.4. We can observe second-order accuracy of the IMPEC2-IPDG methods and third-order accuracy of IMPEC3-IPDG methods with and without the oscillation-free technique. Therefore, the oscillation-free technique does not damp the accuracy in two dimensional case.

Example 3.5.3

Table 3.3
Example 3.5.2: Accuracy test of c for the IMPEC2-IPDG schemes with and without the oscillation-free technique with DIRK(2,2,2).

N	With OF-Tech		No OF-Tech	
	L^2 error	order	L^2 error	order
10	7.08e-2	-	3.46e-2	-
20	1.63e-2	2.16	8.34e-2	2.05
40	4.02e-3	2.02	2.06e-3	2.01
80	1.01e-3	1.99	5.15e-4	2.00
160	2.55e-4	1.99	1.29e-4	2.00

Table 3.4
Example 3.5.2: Accuracy test of c for the IMPEC3-IPDG schemes with and without the oscillation-free technique with DIRK(4,4,3).

N	With OF-Tech		No OF-Tech	
	L^2 error	order	L^2 error	order
10	1.58e-2	-	4.13e-3	-
20	2.05e-3	2.94	6.44e-4	2.68
40	2.71e-4	2.91	1.01e-4	2.68
80	3.30e-5	3.03	1.43e-5	2.81
160	4.11e-6	3.00	2.09e-6	2.77
320	5.34e-7	2.94	3.08e-7	2.76

We take the initial conditions as

$$c(x,y,0) = \begin{cases} 1, & x \le \dfrac{\pi}{2},\ y \le \dfrac{\pi}{2}, \\ 0, & \text{otherwise}, \end{cases} \qquad p(x,y,0) = \cos\left(\frac{x}{2}\right) + \cos\left(\frac{y}{2}\right).$$

Other parameters are choosen as

$$q(x,y,t) = 0,\ z_1 = 1,\ z_2 = 10,\ \mu(c) = \kappa(x,y) = \phi(x,y) = 1,\ \mathbf{D}(\mathbf{u}) = 0.$$

We compute c at terminal time $T = 1.0,\ 5.0$ with $\Delta t = 0.1 \min\{\Delta x, \Delta y\}$ and with

the oscillation-free technique. The results are shown in Fig. 3.1.

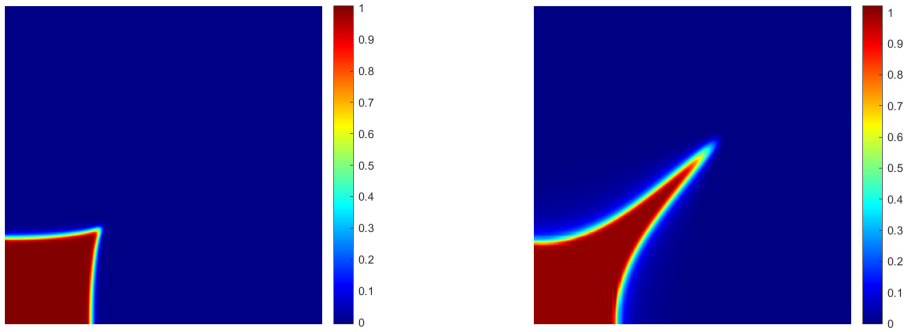

(a) c at T=1.0 (b) c at T=5.0

Figure 3.1 Example 3.5.3: Concentrations c with oscillation-free technique.

From the figure, we can observe that though the bound-preserving technique is missing, the numerical approximations are between 0 and 1. To test the effectiveness of the oscillation-free technique for two dimensional case, we simulate the distributions of c at different time $T = 1.0,\ 5.0$ without oscillation-free technique. The results are given in Fig. 3.2. We can observe that there are some concentration value beyond the lower bound 0 and the upper bound 1.

We also provide simulation of the distributions of c at different time $T = 1.0$ and 15.0, along the diagonal $y = x$ with and without oscillation-free damping term. The results are given in Fig. 3.3. We can observe strong oscillations and physically irrelevant values with overshoot in Fig. 3.3 (b) and undershoot in Fig. 3.3(d), while concentrations c in Fig. 3.3(a) and Fig. 3.3(c) do not, indicating the effectiveness of the oscillation-free technique.

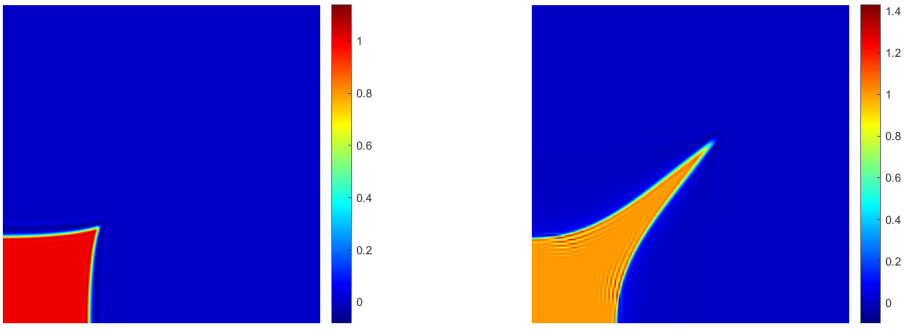

(a) c at T=1.0 (b) c at T=5.0

Figure 3.2 Example 3.5.3: Concentration c without oscillation-free technique.

Example 3.5.4

We choose the initial conditions as

$$c(x, y, 0) = 0.5,\ p(x, y, 0) = 0.$$

Other parameters are taken as

$$z_1 = 0.4,\ z_2 = 0.6,\ \phi(x, y) = 1,\ \mathbf{D}(\mathbf{u}) = 0.1 \begin{pmatrix} |\mathbf{u}| & 0 \\ 0 & |\mathbf{u}| \end{pmatrix}.$$

The injection well is positioned at the upper-right corner of the domain with $q = \frac{1}{\Delta x \Delta y}$ and $\tilde{c} = 1$, and production well is positioned at lower-left corner with $q = -\frac{1}{\Delta x \Delta y}$.

In this example, the diffusion parameter in the concentration equation is set to be

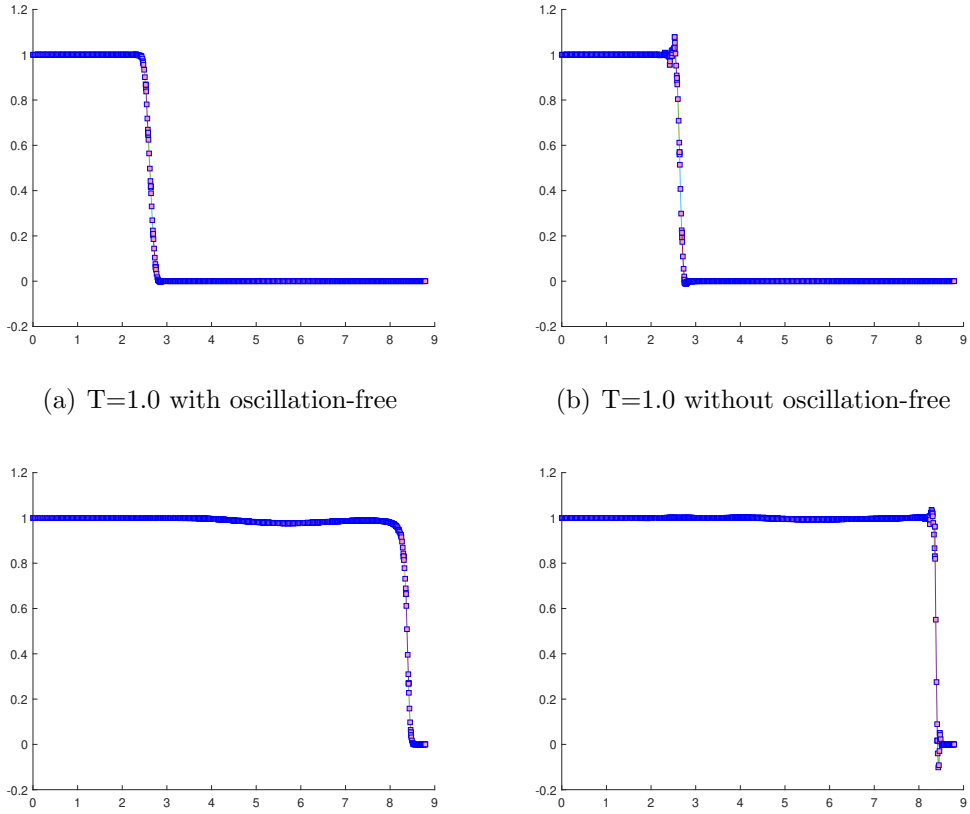

(a) T=1.0 with oscillation-free

(b) T=1.0 without oscillation-free

(c) T=15.0 with oscillation-free

(d) T=15.0 without oscillation-free

Figure 3.3 Example 3.5.3: Concentration c with and without oscillation-free technique along the diagonal $y = x$.

more practical. We choose $\Delta t = 0.005 \min\{\Delta x, \Delta y\}$, $N_x = N_y = 40$ and terminal time $T = 1,\ 5,\ 10,\ 15$. The simulations are shown in Fig. 3.4. We can see that all the numerical approximations of c are in the desired bound between 0 and 1. Therefore, the oscillation-free technique works for the petroleum production simulations.

Example 3.5.5

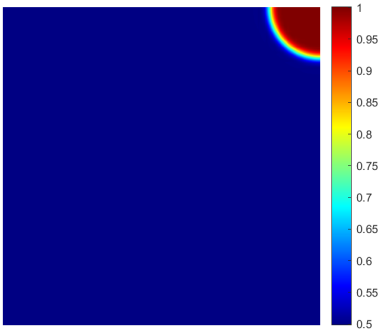

(a) c at T=1

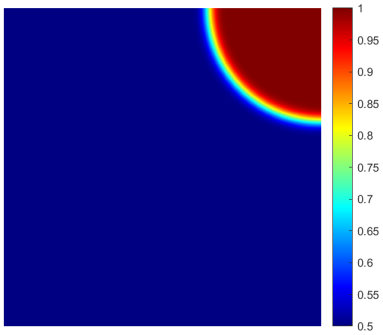

(b) c at T=5

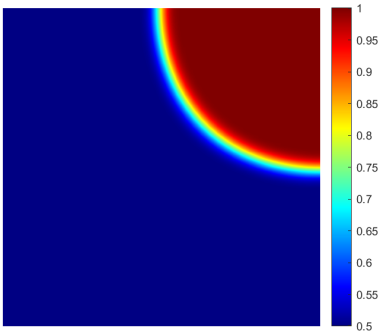

(c) c at T=10

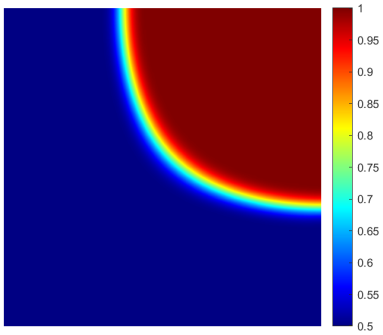

(d) c at T=15

Figure 3.4 Example 3.5.4: Concentration c at different time with IMPEC3-OFDG.

We choose the initial conditions as

$$c(x, y, 0) = 0,\ p(x, y, 0) = 0.$$

Other parameters are taken as

$$z_1 = 0.001,\ z_2 = 0.001,\ \phi(x, y) = 1,\ \mathbf{D}(\mathbf{u}) = 0.01 \begin{pmatrix} |\mathbf{u}| & 0 \\ 0 & |\mathbf{u}| \end{pmatrix}.$$

Permeability and viscosity are

$$\kappa(x,y) = 1 + 10^{-2}\cos(10\pi x)\cos(10\pi y),\ \mu(c) = e^{6(1-c)}.$$

There is a perturbation of the permeability to create the onset of the fingers. The injection well is positioned at the upper-right corner of the domain with $q = \frac{1}{\Delta x \Delta y}$ and $\tilde{c} = 1$, and production well is positioned at lower-left corner with $q = -\frac{1}{\Delta x \Delta y}$. We set $\Delta t = 0.005 \min\{\Delta x, \Delta y\}$ and terminal time $T = 1,\ 5,\ 9$. The simulations by using IMPEC3 and under the coarse mesh $N_x = N_y = 80$ and refined mesh $N_x = N_y = 100$ are shown in Fig. 3.5. Comparing the coarse mesh with the refined mesh, we observe that the fingering pattern maintains a similar shape at corresponding spots in both meshes. This indicates that the grid sensitivity is effectively managed through the use of the IMPEC3-OFDG method.

Example 3.5.6

Based on 3.5.5, we choose the permeability

$$\kappa(x,y) = 1 + 10^{-2}\cos(50\pi x)\cos(50\pi y)$$

to generate more fingerings with refined mesh $N_x = N_y = 100$ and terminal time $T = 1,\ 4,\ 8,\ 11$. The simulations using the IMPEC2 method with $\mathcal{Q}^1$ polynomials

and IMPEC3 method with $\mathcal{Q}^2$ polynomials are depicted in Figs. 3.6 and 3.7, respectively. We observe the smooth generation of viscous fingering over time, with all concentration values remaining within the physically relevant range of 0 to 1, exhibiting minimal overshoot and undershoot. Fig. 3.6 shows four fingers, while Fig. 3.7 shows six fingers. This comparison illustrates the numerical artifacts in simulating viscous fingering. The high order numerical methods produce more accurate simulations with detailed fingerings. Therefore, high order methods are preferable to reduce the numerical artifacts.

We also provide simulations of the viscous fingering phenomenon with an obstacle in Fig. 3.9. The obstacle problem setup is described in Fig. 3.8. The obstacle is an impermeable area with yellow rocks at the lower-right part of the region in Fig. 3.8. In the surrounding matrix, the permeability is defined as $\kappa(x, y) = 1 + 10^{-2}\cos(50\pi x)\cos(50\pi y)$, viscosity depends on the concentration is $\mu(c) = e^{6(1-c)}$, the porosity $\phi = 1$, and the parameters of the diffusion-dispersion are given

$$d_{mol} = 2.55 \times 10^{-9}, d_{long} = d_{tran} = 0.$$

The mobility ratio (the ratio = viscosity of residing fluid/viscosity of the solvent) is 20. The injection well is positioned at the upper-right corner of the domain with $q = \frac{1}{\Delta x \Delta y}$ and $\tilde{c} = 1$, and production well is positioned at lower-left corner with $q = -\frac{1}{\Delta x \Delta y}$. The viscous fingers are generated by randomly perturbing the permeability. The

simulation is performed using a 100×100 grid with $\mathcal{Q}^2$ polynomials. Snapshots at $t = 1, 5, 10, 11$ of concentration contours are shown in Fig. 3.9. We observe in Fig. 3.9 that the estimated smooth growth of the fingering over time with physically relevant values in the desired bound, and the flow path does not pass the obstacle.

3.6 Concluding remarks

In this paper, we presented the OFDG methods for simulating two-component compressible displacements in porous media with IMPEC time discretization. By incorporating the oscillation-free damping term in two space dimensions, we achieved physically relevant numerical approximations. The use of the IMPEC time marching method ensures the maintenance of high-order accuracy. Numerical experiments demonstrated the effectiveness of the oscillation-free technique in simulating viscous fingering instability phenomena with obstacles. Our proposed high-order numerical scheme significantly reduces the sensitivity of mesh orientation, highlighting its efficiency. Additionally, we provided a comparison of numerical tests between the lower order and higher order methods to demonstrate the necessity of the higher order scheme.

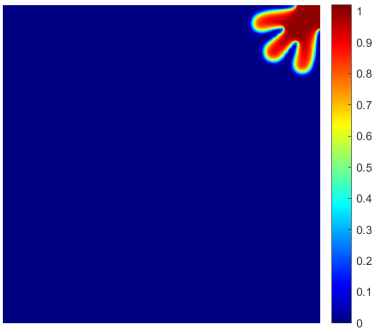

(a) c at T=1

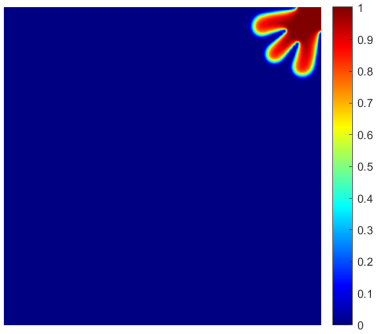

(b) c at T=1

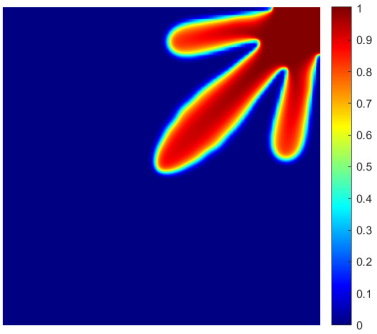

(c) c at T=5

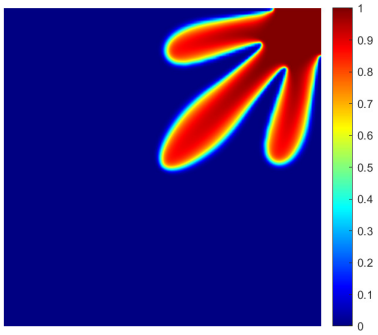

(d) c at T=5

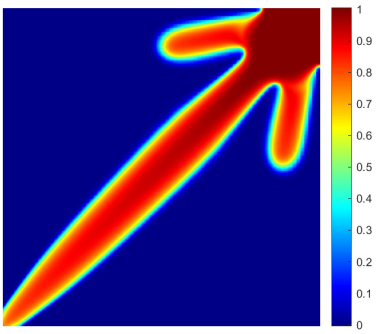

(e) c at T=9

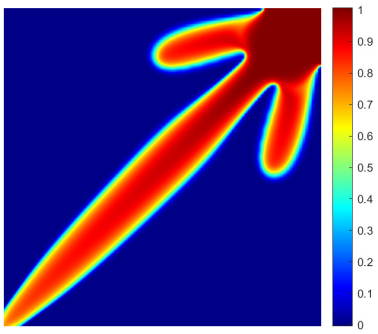

(f) c at T=9

Figure 3.5 Example 3.5.5: Concentration c of viscous fingering phenomenon with IMPEC3-OFDG in $\mathcal{Q}_2$ under the coarse mesh(Left) and refined mesh(Right).

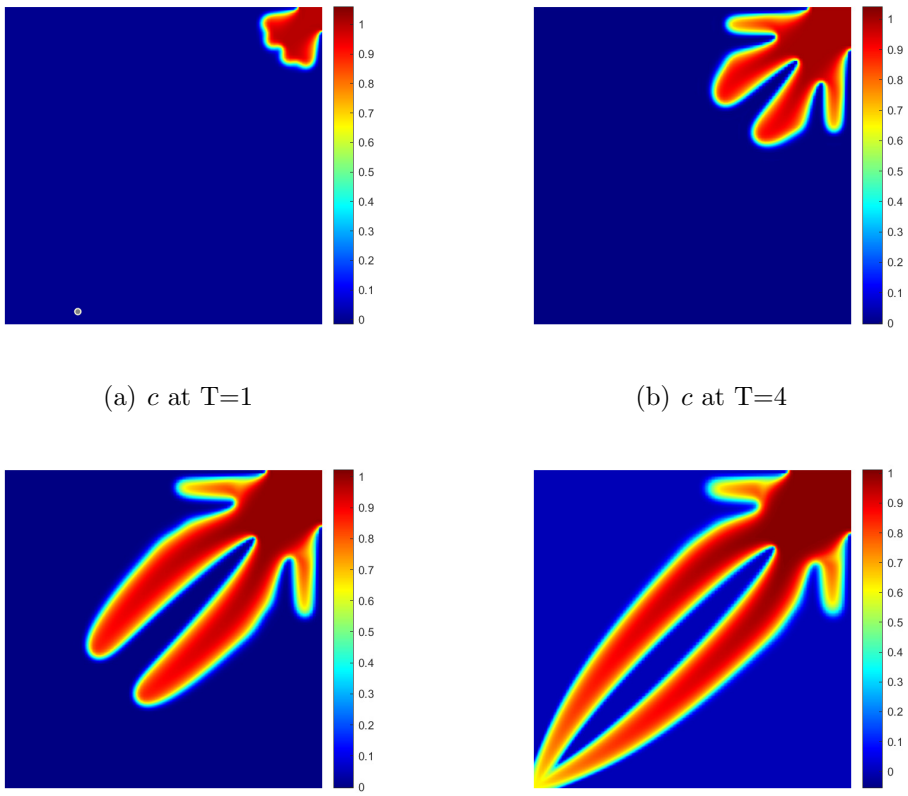

(a) c at T=1

(b) c at T=4

(c) c at T=8

(d) c at T=11

Figure 3.6 Example 3.5.6: Concentration c with IMPEC2-OFDG in $\mathcal{Q}^1$.

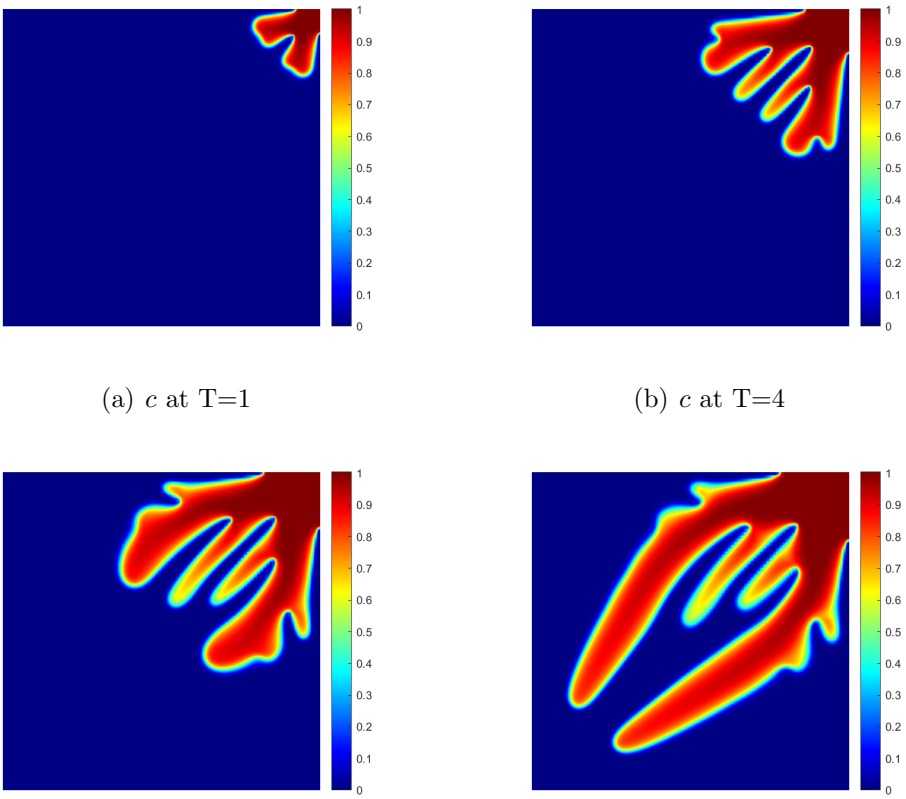

(a) c at T=1

(b) c at T=4

(c) c at T=8

(d) c at T=11

Figure 3.7 Example 3.5.6:Concentration c of with IMPEC3-OFDG in $\mathcal{Q}^2$.

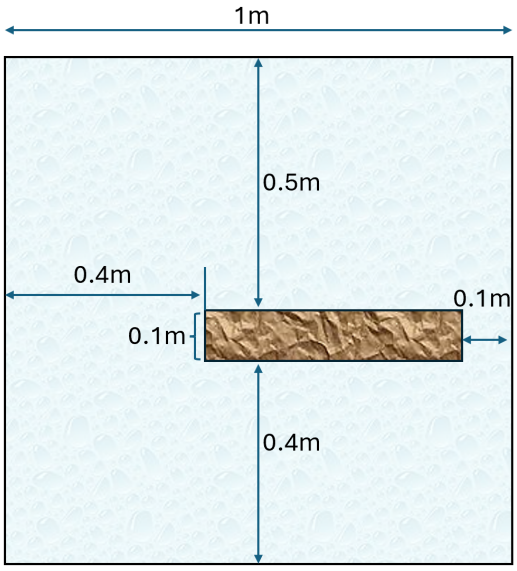

Figure 3.8 Obstacle problem setup

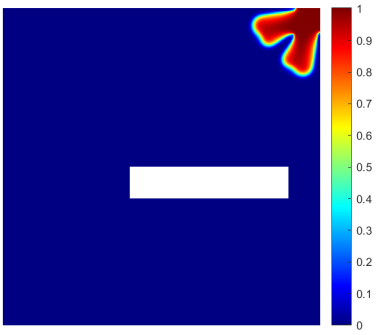

(a) c at T=1

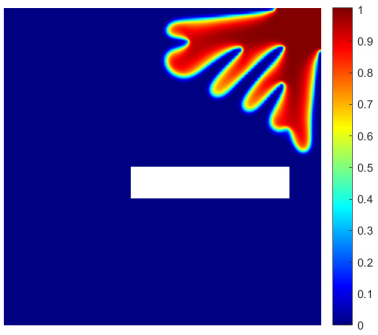

(b) c at T=5

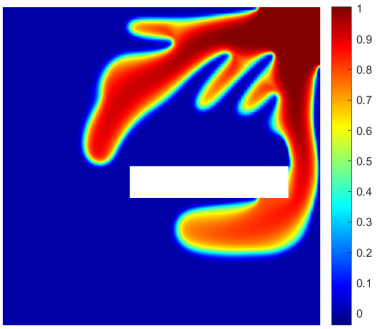

(c) c at T=10

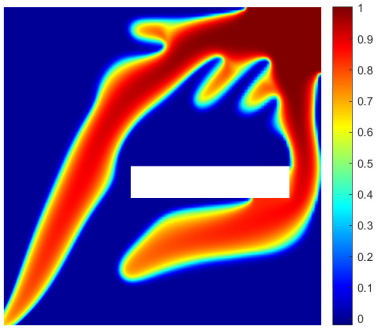

(d) c at T=11

Figure 3.9 Example 3.5.6: Concentration c of Viscous Fingering phenomenon at different time with oscillation-free technique with obstacle.

Chapter 4

Conclusion

This dissertation has explored the application of discontinuous Galerkin (DG) methods to the system of compressible miscible displacements, particularly in the context of modeling surfactant flooding in enhanced oil recovery (EOR) techniques. While DG methods are generally effective in simulating most problems in miscible displacements, they can encounter issues, such as oscillations in numerical results, particularly in tricky problem settings, leading to nonphysical numerical approximations.

To address these challenges, this work first introduced a bound-preserving Discontinuous Galerkin method with Second-order Implicit Pressure Explicit Concentration (SIPEC) time marching method. This approach was used to compute the system of two-component compressible miscible displacements in porous media.

Moreover, to efficiently simulate viscous fingering phenomena, a higher-order discontinuous Galerkin method for the coupled nonlinear system of compressible miscible displacements was proposed. This method adopted the Implicit Pressure Explicit Concentration time marching approach (IMPEC) based on the implicit-explicit Runge-Kutta (IMEX-RK) Butcher tableau to achieve high-order temporal accuracy while ensuring stability. Furthermore, we introduced an oscillation-free damping term to suppress spurious oscillations near the discontinuity in high-order DG methods.

Numerical experiments showed that the incorporation of bound-preserving DG method with SIPEC time marching and high-order OFDG with IMPEC time marching yielded satisfactory results for simulating fluid flow in reservoirs. Overall, the research in this dissertation contributes to the advancement of numerical methods for simulating complex fluid flow phenomena in porous media, particularly in the context of EOR applications.

Bibliography

[1] Ewing RE, Wheeler MF, et al. A time-discretization procedure for a mixed finite element approximation of miscible displacement in porous media. RAIRO Analyse numérique. 1983;17(3):249-65.

[2] Ewing RE, Wheeler MF, et al. The approximation of the pressure by a mixed method in the simulation of miscible displacement. RAIRO Analyse numérique. 1983;17(1):17-33.

[3] Douglas J, Roberts JE. Numerical methods for a model for compressible miscible displacement in porous media. Mathematics of Computation. 1983;41(164):441-59.

[4] Yuan Y. The characteristic finite difference fractional steps methods for compressible two-phase displacement problem. Science in China Series A: Mathematics. 1999;42:48-57.

[5] Yang D. A splitting positive definite mixed element method for miscible displacement of compressible flow in porous media. Numerical Methods for Partial Differential Equations: An International Journal. 2001;17(3):229-49.

[6] Wang H, Liang D, Ewing RE, Lyons SL, Qin G. An accurate approximation to compressible flow in porous media with wells. In: Numerical Treatment of Multiphase Flows in Porous Media: Proceedings of the International Workshop Held a Beijing, China, 2–6 August 1999. Springer; 2000. p. 324-32.

[7] Wang H, Liang D, Ewing RE, Lyons SL, Qin G. An approximation to miscible fluid flows in porous media with point sources and sinks by an Eulerian–Lagrangian localized adjoint method and mixed finite element methods. SIAM Journal on Scientific Computing. 2000;22(2):561-81.

[8] Kumar S. A mixed and discontinuous Galerkin finite volume element method for incompressible miscible displacement problems in porous media. Numerical Methods for Partial Differential Equations. 2012;28(4):1354-81.

[9] Chainais-Hillairet C, Krell S, Mouton A. Convergence analysis of a DDFV scheme for a system describing miscible fluid flows in porous media. Numerical Methods for Partial Differential Equations. 2015;31(3):723-60.

[10] Cui M. A combined mixed and discontinuous Galerkin method for compressible miscible displacement problem in porous media. Journal of computational and applied mathematics. 2007;198(1):19-34.

[11] Cui M. Analysis of a semidiscrete discontinuous Galerkin scheme for compressible miscible displacement problem. Journal of computational and applied mathematics. 2008;214(2):617-36.

[12] Yang J, Chen Y. A priori error estimates of a combined mixed finite element and discontinuous Galerkin method for compressible miscible displacement with molecular diffusion and dispersion. Journal of Computational Mathematics. 2011:91-107.

[13] Yang J, Chen Y. A priori error analysis of a discontinuous Galerkin approximation for a kind of compressible miscible displacement problems. Science China Mathematics. 2010;53:2679-96.

[14] Yu F, Guo H, Chuenjarern N, Yang Y. Conservative local discontinuous Galerkin method for compressible miscible displacements in porous media. Journal of Scientific Computing. 2017;73:1249-75.

[15] Bartels S, Jensen M, Müller R. Discontinuous Galerkin finite element convergence for incompressible miscible displacement problems of low regularity. SIAM Journal on Numerical Analysis. 2009;47(5):3720-43.

[16] Guo H, Zhang Q, Yang Y. A combined mixed finite element method and local discontinuous Galerkin method for miscible displacement problem in porous media. Science China Mathematics. 2014;57:2301-20.

[17] Rivière B. Discontinuous Galerkin methods for solving elliptic and parabolic equations: theory and implementation. SIAM; 2008.

[18] Sun S, Riviere B, Wheeler MF. A combined mixed finite element and discontinuous Galerkin method for miscible displacement problem in porous media. In: Recent Progress in Computational and Applied PDES: Conference Proceedings for the International Conference Held in Zhangjiajie in July 2001. Springer; 2002. p. 323-51.

[19] Wheeler MF, Darlow BL. Interior penalty Galerkin procedures for miscible displacement problems in porous media. In: Computational methods in nonlinear mechanics (Proc. Second Internat. Conf., Univ. Texas, Austin, Tex., 1979); 1980. p. 485-506.

[20] Lee S, Lee YJ, Wheeler MF. A locally conservative enriched Galerkin approximation and efficient solver for elliptic and parabolic problems. SIAM Journal on Scientific Computing. 2016;38(3):A1404-29.

[21] Zhang Y, Zhang X, Shu CW. Maximum-principle-satisfying second order discontinuous Galerkin schemes for convection–diffusion equations on triangular meshes. Journal of Computational Physics. 2013;234:295-316.

[22] Li XH, Shu CW, Yang Y. Local discontinuous Galerkin method for the Keller-Segel chemotaxis model. Journal of Scientific Computing. 2017;73(2-3):943-67.

[23] Guo H, Yang Y. Bound-preserving discontinuous Galerkin method for compressible miscible displacement in porous media. SIAM Journal on Scientific Computing. 2017;39(5):A1969-90.

[24] Du J, Yang Y. Maximum-principle-preserving third-order local discontinuous Galerkin method for convection-diffusion equations on overlapping meshes. Journal of computational physics. 2019;377:117-41.

[25] Chen Z, Huang H, Yan J. Third order maximum-principle-satisfying direct discontinuous Galerkin methods for time dependent convection diffusion equations on unstructured triangular meshes. Journal of Computational Physics. 2016;308:198-217.

[26] Srinivasan S, Poggie J, Zhang X. A positivity-preserving high order discontinuous Galerkin scheme for convection–diffusion equations. Journal of Computational Physics. 2018;366:120-43.

[27] Guo L, Yang Y. Positivity preserving high-order local discontinuous Galerkin method for parabolic equations with blow-up solutions. Journal of Computational Physics. 2015;289:181-95.

[28] Xiong T, Qiu JM, Xu Z. High order maximum-principle-preserving discontinuous Galerkin method for convection-diffusion equations. SIAM Journal on Scientific Computing. 2015;37(2):A583-608.

[29] Chuenjarern N, Xu Z, Yang Y. High-order bound-preserving discontinuous Galerkin methods for compressible miscible displacements in porous media on triangular meshes. Journal of Computational Physics. 2019;378:110-28.

[30] Guo H, Liu X, Yang Y. High-order bound-preserving finite difference methods for miscible displacements in porous media. Journal of Computational Physics. 2020;406:109219.

[31] Xu Z, Yang Y, Guo H. High-order bound-preserving discontinuous Galerkin methods for wormhole propagation on triangular meshes. Journal of Computational Physics. 2019;390:323-41.

[32] Du J, Wang C, Qian C, Yang Y. High-order bound-preserving discontinuous Galerkin methods for stiff multispecies detonation. SIAM Journal on Scientific Computing. 2019;41(2):B250-73.

[33] Du J, Yang Y. Third-order conservative sign-preserving and steady-state-preserving time integrations and applications in stiff multispecies and multi-reaction detonations. Journal of Computational Physics. 2019;395:489-510.

[34] Shu CW. Total-variation-diminishing time discretizations. SIAM Journal on Scientific and Statistical Computing. 1988;9(6):1073-84.

[35] Shu CW, Osher S. Efficient implementation of essentially non-oscillatory shock-capturing schemes. Journal of computational physics. 1988;77(2):439-71.

[36] Gottlieb S, Shu CW, Tadmor E. Strong stability-preserving high-order time discretization methods. SIAM review. 2001;43(1):89-112.

[37] Gottlieb S, Ketcheson DI, Shu CW. High order strong stability preserving time discretizations. Journal of Scientific Computing. 2009;38(3):251-89.

[38] Xu Z, Yang Y. The hybrid dimensional representation of permeability tensor: a reinterpretation of the discrete fracture model and its extension on nonconforming meshes. Journal of Computational Physics. 2020;415:109523.

[39] Monteagudo J, Firoozabadi A. Comparison of fully implicit and IMPES formulations for simulation of water injection in fractured and unfractured media. International journal for numerical methods in engineering. 2007;69(4):698-728.

[40] Zidane A, Firoozabadi A. An implicit numerical model for multicomponent compressible two-phase flow in porous media. Advances in Water Resources. 2015;85:64-78.

[41] Moortgat J. Adaptive implicit finite element methods for multicomponent compressible flow in heterogeneous and fractured porous media. Water Resources Research. 2017;53(1):73-92.

[42] Hoteit H, Firoozabadi A. Multicomponent fluid flow by discontinuous Galerkin and mixed methods in unfractured and fractured media. Water Resources Research. 2005;41(11).

[43] Chen Z, Huan G, Ma Y. Computational methods for multiphase flows in porous media. SIAM; 2006.

[44] Chen Z. Reservoir simulation: mathematical techniques in oil recovery. SIAM; 2007.

[45] Zidane A, Firoozabadi A. An efficient numerical model for multicomponent compressible flow in fractured porous media. Advances in water resources. 2014;74:127-47.

[46] Sheldon J, Cardwell Jr W. One-dimensional, incompressible, noncapillary, two-phase fluid flow in a porous medium. Transactions of the AIME. 1959;216(01):290-6.

[47] Stone H, Garder Jr A. Analysis of gas-cap or dissolved-gas drive reservoirs. Society of Petroleum Engineers Journal. 1961;1(02):92-104.

[48] Chen H, Fan X, Sun S. A fully mass-conservative iterative IMPEC method for multicomponent compressible flow in porous media. Journal of Computational and Applied Mathematics. 2019;362:1-21.

[49] Chertock A, Cui S, Kurganov A, Wu T. Steady state and sign preserving semi-implicit Runge–Kutta methods for ODEs with stiff damping term. SIAM Journal on Numerical Analysis. 2015;53(4):2008-29.

[50] Feng W, Guo H, Kang Y, Yang Y. Bound-preserving discontinuous Galerkin methods with second-order implicit pressure explicit concentration time marching for compressible miscible displacements in porous media. Journal of Computational Physics. 2022;463:111240.

[51] Feng W, Guo H, Tian L, Yang Y. Sign-preserving second-order IMPEC time discretization and its application in compressible miscible displacement with Darcy-Forchheimer models. Journal of Computational Physics. 2023;474:111775.

[52] Shu CW. Discontinuous Galerkin methods: general approach and stability. Numerical solutions of partial differential equations. 2009;201.

[53] Qiu J, Shu CW. Runge–Kutta discontinuous Galerkin method using WENO limiters. SIAM Journal on Scientific Computing. 2005;26(3):907-29.

[54] Zhong X, Shu CW. A simple weighted essentially nonoscillatory limiter for Runge–Kutta discontinuous Galerkin methods. Journal of Computational Physics. 2013;232(1):397-415.

[55] Hiltebrand A, Mishra S. Entropy stable shock capturing space–time discontinuous Galerkin schemes for systems of conservation laws. Numerische Mathematik. 2014;126:103-51.

[56] Lu J, Liu Y, Shu CW. An oscillation-free discontinuous Galerkin method for scalar hyperbolic conservation laws. SIAM Journal on Numerical Analysis. 2021;59(3):1299-324.

[57] Du J, Liu Y, Yang Y. An Oscillation-Free Bound-Preserving Discontinuous Galerkin Method for Multi-component Chemically Reacting Flows. Journal of Scientific Computing. 2023;95(3):90.

[58] Boscarino S, Qiu JM, Russo G, Xiong T. A high order semi-implicit IMEX WENO scheme for the all-Mach isentropic Euler system. Journal of Computational Physics. 2019;392:594-618.

[59] Chou SH, Li Q. Mixed finite element methods for compressible miscible displacement in porous media. mathematics of computation. 1991;57(196):507-27.

[60] Yuan Y. The upwind finite difference fractional steps methods for two-phase compressible flow in porous media. Numerical Methods for Partial Differential Equations: An International Journal. 2003;19(1):67-88.

[61] Yuan Yr. The modified upwind finite difference fractional steps method for compressible two-phase displacement problem. Acta Mathematicae Applicatae Sinica. 2004;20(3):381-96.

[62] Ma N, Yang D, Lu T. L2-norm error bounds of characteristics collocation method for compressible miscible displacement in porous media. International Journal of Numerical Analysis and Modeling. 2005;2:28-42.

[63] Chen HZ, Wang H. An optimal-order error estimate on an H1-Galerkin mixed

method for a nonlinear parabolic equation in porous medium flow. Numerical Methods for Partial Differential Equations: An International Journal. 2010;26(1):188-205.

[64] Yang J. A posteriori error of a discontinuous Galerkin scheme for compressible miscible displacement problems with molecular diffusion and dispersion. International journal for numerical methods in fluids. 2011;65(7):781-97.

[65] Guo H, Zhang Q, Wang J. Error analysis of the semi-discrete local discontinuous Galerkin method for compressible miscible displacement problem in porous media. Applied Mathematics and Computation. 2015;259:88-105.

[66] Riviè; re B, Wheeler MF, Banaś K. Part II. Discontinuous Galerkin method applied to a single phase flow in porous media. Computational Geosciences. 2000;4:337-49.

[67] Sun S, Wheeler MF. Discontinuous Galerkin methods for coupled flow and reactive transport problems. Applied Numerical Mathematics. 2005;52(2-3):273-98.

[68] Reed W, Hill T. Triangular mesh methods forthe neutron transport equation, Los Alamos ScientificLaboratory Report LA-UR-73-479, Los Alamos, NMRemacle JF, Flaherty J, Shephard M. 2003. An adaptivediscontinuous Galerkin technique with an orthogonal ba-sis applied to Rayleigh-Taylor flow instabilities. SIAM Review. 1973;45:53-72.

[69] Zhang X, Shu CW. On maximum-principle-satisfying high order schemes for scalar conservation laws. Journal of Computational Physics. 2010;229(9):3091-120.

[70] Zhang X, Shu CW. On positivity-preserving high order discontinuous Galerkin schemes for compressible Euler equations on rectangular meshes. Journal of Computational Physics. 2010;229(23):8918-34.

[71] Zhang X, Shu CW. Positivity-preserving high order discontinuous Galerkin schemes for compressible Euler equations with source terms. Journal of Computational Physics. 2011;230(4):1238-48.

[72] Yang Y, Shu CW. Discontinuous Galerkin method for hyperbolic equations involving-singularities: negative-order norm error estimates and applications. Numerische Mathematik. 2013;124(4):753-81.

[73] Yang Y, Wei D, Shu CW. Discontinuous Galerkin method for Krause's consensus models and pressureless Euler equations. Journal of Computational Physics. 2013;252:109-27.

[74] Zhao X, Yang Y, Seyler CE. A positivity-preserving semi-implicit discontinuous Galerkin scheme for solving extended magnetohydrodynamics equations. Journal of Computational Physics. 2014;278:400-15.

[75] Qin T, Shu CW, Yang Y. Bound-preserving discontinuous Galerkin methods for relativistic hydrodynamics. Journal of Computational Physics. 2016;315:323-47.

[76] Xing Y, Zhang X, Shu CW. Positivity-preserving high order well-balanced discontinuous Galerkin methods for the shallow water equations. Advances in Water Resources. 2010;33(12):1476-93.

[77] Zhang Y, Zhang X, Shu CW. Maximum-principle-satisfying second order discontinuous Galerkin schemes for convection–diffusion equations on triangular meshes. Journal of Computational Physics. 2013;234:295-316.

[78] Du J, Yang Y. Maximum-principle-preserving third-order local discontinuous Galerkin method for convection-diffusion equations on overlapping meshes. Journal of computational physics. 2019;377:117-41.

[79] Srinivasan S, Poggie J, Zhang X. A positivity-preserving high order discontinuous Galerkin scheme for convection–diffusion equations. Journal of Computational Physics. 2018;366:120-43.

[80] Guo L, Yang Y. Positivity preserving high-order local discontinuous Galerkin method for parabolic equations with blow-up solutions. Journal of Computational Physics. 2015;289:181-95.

[81] Chertock A, Cui S, Kurganov A, Wu T. Steady state and sign preserving semi-implicit Runge–Kutta methods for ODEs with stiff damping term. SIAM Journal on Numerical Analysis. 2015;53(4):2008-29.

[82] Sun S, Wheeler MF. Symmetric and nonsymmetric discontinuous Galerkin methods for reactive transport in porous media. SIAM Journal on Numerical Analysis. 2005;43(1):195-219.

[83] Paterson L. Radial fingering in a Hele Shaw cell. Journal of Fluid Mechanics. 1981;113:513-29.

[84] Saffman PG, Taylor GI. The penetration of a fluid into a porous medium or Hele-Shaw cell containing a more viscous liquid. Proceedings of the Royal Society of London Series A Mathematical and Physical Sciences. 1958;245(1242):312-29.

[85] Homsy GM. Viscous fingering in porous media. Annual review of fluid mechanics. 1987;19(1):271-311.

[86] Yuan Y. The characteristic finite difference fractional steps methods for compressible two-phase displacement problem. Science in China Series A: Mathematics. 1999;42:48-57.

[87] Riviere B. Discontinuous Galerkin methods for solving the miscible displacement problem in porous media. The University of Texas at Austin; 2000.

[88] Du J, Wang C, Qian C, Yang Y. High-order bound-preserving discontinuous Galerkin methods for stiff multispecies detonation. SIAM Journal on Scientific Computing. 2019;41(2):B250-73.

[89] Du J, Yang Y. Third-order conservative sign-preserving and steady-state-preserving time integrations and applications in stiff multispecies and multi-reaction detonations. Journal of Computational Physics. 2019;395:489-510.

[90] Xu Z, Huang Z, Yang Y. The hybrid-dimensional Darcy's law: a non-conforming reinterpreted discrete fracture model (RDFM) for single-phase flow in fractured media. Journal of Computational Physics. 2023;473:111749.

[91] Zidane A, Firoozabadi A. An efficient numerical model for multicomponent compressible flow in fractured porous media. Advances in water resources. 2014;74:127-47.

[92] Liu Y, Lu J, Shu CW. An essentially oscillation-free discontinuous Galerkin method for hyperbolic systems. SIAM Journal on Scientific Computing. 2022;44(1):A230-59.

[93] Bear J. Dynamics of fluids in porous media. Courier Corporation; 2013.

[94] Ascher UM, Ruuth SJ, Spiteri RJ. Implicit-explicit Runge-Kutta methods for time-dependent partial differential equations. Applied Numerical Mathematics. 1997;25(2-3):151-67.

[95] Boscarino S, Qiu JM, Russo G, Xiong T. A high order semi-implicit IMEX WENO scheme for the all-Mach isentropic Euler system. Journal of Computational Physics. 2019;392:594-618.

Appendix A

Copyright permission

Copyright

Overview

In order for Elsevier to publish and disseminate research articles, we need certain publishing rights from authors, which are determined by a publishing agreement between the author and Elsevier.

For articles published open access, the authors license exclusive rights in their article to Elsevier where a CC BY-NC-ND end user license is selected, and license non-exclusive rights where a CC BY end user license is selected.

For articles published under the subscription model, the authors typically transfer copyright to Elsevier. In some circumstances, authors may instead grant us (or the learned society for whom we publish) an exclusive license to publish and disseminate their work.

Regardless of whether they choose to publish open access or subscription with Elsevier, authors have many of the same rights under our publishing agreement, which support their need to share, disseminate and maximize the impact of their research.

For open access articles, authors will also have additional rights, depending on the Creative Commons end user license that they select. This Creative Commons license sets out the rights that readers (as well as the authors) have to re-use and share the article. Learn how articles can be re-used and shared under these licenses.

This page aims to summarize authors' rights when publishing with Elsevier; these are explained in more detail in the publishing agreement between the author and Elsevier.

Irrespective of how an article is published, Elsevier is committed to protect and defend authors' works and their reputation. We take allegations of infringement, plagiarism, ethical disputes, and fraud very seriously.

Author rights

The below table explains the rights that authors have when they publish with Elsevier, for authors who choose to publish either open access or subscription. These apply to the corresponding author and all co-authors.

Author rights in Elsevier's proprietary journals	**Published open access**	**Published subscription**
Retain patent and trademark rights	√	√
Retain the rights to use their research data freely without any restriction	√	√
Receive proper attribution and credit for their published work	√	√
Re-use their own material in new works without permission or payment (with full acknowledgement of the original article): 1. Extend an article to book length	√	√

2. Include an article in a subsequent compilation of their own work 3. Re-use portions, excerpts, and their own figures or tables in other works.		
Use and share their works for scholarly purposes (with full acknowledgement of the original article): 1. In their own classroom teaching. Electronic and physical distribution of copies is permitted 2. If an author is speaking at a conference, they can present the article and distribute copies to the attendees 3. Distribute the article, including by email, to their students and to research colleagues who they know for their personal use 4. Share and publicize the article via Share Links, which offers 50 days' free access for anyone, without signup or registration 5. Include in a thesis or dissertation (provided this is not published commercially) 6. Share copies of their article privately as part of an invitation-only work group on commercial sites with which the publisher has a hosting agreement	√	√
Publicly share the preprint on any website or repository at any time.	√	√
Publicly share the accepted manuscript on non-commercial sites	√	√ using a CC BY-NC-ND license and usually only after an embargo period (see Sharing Policy for more information)

Publicly share the final published article	√ in line with the author's choice of end user license	×
Retain copyright	√	×

Institution rights

Regardless of how the author chooses to publish with Elsevier, their institution has the right to use articles for classroom teaching and internal training. Articles can be used for these purposes throughout the author's institution, not just by the author:

Institution rights in Elsevier's proprietary journals (providing full acknowledgement of the original article is given)	**All articles**
Copies can be distributed electronically as well as in physical form for classroom teaching and internal training purposes	√
Material can be included in coursework and courseware programs for use within the institution (but not in Massive Open Online Courses)	√
Articles can be included in applications for grant funding	√
Theses and dissertations which contain embedded final published articles as part of the formal submission can be posted publicly by the awarding institution with DOI links back to the formal publication on	√

Government rights

For US government employees, works created within the scope of their employment are considered to be public domain and Elsevier's publishing agreements do not require a transfer or license of rights for such works.

In the UK and certain commonwealth countries, a work created by a government employee is copyrightable, but the government may own the copyright (Crown copyright). Please find information about UK government employees publishing open access.

Find out more

- Download a sample publishing agreement for articles financed by journal subscriptions in English and French
- Download a sample publishing agreement for articles published open access with a commercial user license (CC BY) in English and French.
- Download a sample publishing agreement for articles published open access with a non-commercial user license (CC BY-NC-ND) in English and French.
- Download a sample publishing agreement for articles published open access with a non-commercial user license (CC BY-NC) in English and French.
- For authors who wish to self-archive see our sharing guidelines
- See our author pages for further details about how to promote your article
- See our hosting page for additional information on hosting research published by Elsevier
- For use of Elsevier material not defined here please see our permissions page or visit the Permissions Support Center
- If an author has become aware of a possible plagiarism, fraud or infringement we recommend contacting their Elsevier publishing contact who can then liaise with our in-house legal department
- If you are publishing in a society or third party owned journal, they may have different publishing agreements. Please see the journal's Guide for Authors for journal specific

copyright information